

# Turbulence evolution and mixing in a two-layer stably stratified fluid

By PABLO HUQ<sup>1</sup> AND REX E. BRITTER<sup>2</sup>

<sup>1</sup> College of Marine Studies, University of Delaware, Newark, Delaware 19716, USA

<sup>2</sup> Department of Engineering, University of Cambridge, Cambridge CB2 1PZ, UK

(Received 25 October 1989 and in revised form 18 May 1994)

The results of an experimental study of shear-free decaying grid-generated turbulence on both sides of a sharp interface between two homogeneous layers of different densities are presented. The evolution of turbulence and mixing were examined by simultaneously mapping the velocity ( $u, w$ ) and density fields ( $\rho$ ) and the vertical mass flux  $F(= \overline{\rho w} / \rho' w')$  together with flow visualization in a low-noise water tunnel. Buoyancy was induced by salinity differences so the value of the Schmidt number  $S_c = 700$ . Density stratification altered the inertial–buoyancy force balance (most simply expressed by  $Nt$ , the product of the buoyancy frequency  $N$  and turbulent timescale  $t$ ) so as to attenuate turbulent velocity fluctuations, vertical motions and interfacial convolutions, normalized density fluctuations, vertical flux mass, and mean interfacial thickness. Vertical velocity fluctuations  $w'$  were found to increase with distance from the interface, whereas the  $u'$ -distribution can be non-monotonic. The maximum value of the mass flux,  $F$ , was found to be about 0.5 which was less than the typical value of 0.7 for thermally stratified wind tunnel experiments for which  $S_c = 0.7$ . The vertical mass flux can be a combination of down-gradient and counter-gradient transport with the ratio varying with  $Nt$  (e.g. at  $Nt \approx 5$ , the flux is counter-gradient). The flux Richardson number  $R_f$  was found to increase monotonically to values of approximately 0.05.

---

## 1. Introduction

Increased levels of pollution globally have been accompanied by growing public concern about the quality of the environment. Therefore there is a need for quantitative assessment of the hazards associated with the release of effluents. Though the estimation of concentration levels, and hence mixing, is a significant component in the evolution of hazards, there is a lack of understanding of turbulent mixing processes, particularly those in stratified environments. Density stratification (e.g. arising from variations of temperature and salinity in lakes, estuaries and oceans, or from temperature and humidity in the atmosphere) can influence mixing profoundly; for example, strong stable stratification inhibits vertical motions and retards mixing. Stable stratification influences the turbulent field because energy is depleted by work against gravity (Turner 1973). Thus, the problem of turbulence and mixing in a density-stratified fluid is complex: it is dependent on the interaction of two dynamic scales, one due to mechanical turbulence and the other from the buoyancy of the density field.

Previous efforts to understand mixing processes in density-stratified fluids have focused on the evolution of decaying grid-generated turbulence in a linearly stratified fluid column. To study this configuration, experiments were conducted in water tunnels

by Van Atta and co-workers (e.g. Itsweire, Helland & Van Atta 1986) as well as in wind tunnels by Lienhard & Van Atta (1990) and Yoon & Warhaft (1990). These experiments established that the vertical mass transport diminishes to zero on a timescale of the order of the inverse of the buoyancy frequency,  $N$ , of the density gradient. For the water tunnel experiments the density gradient was generated by salinity variations. In contrast, the stratification in wind tunnels was due to temperature gradients. The ratio of the diffusivity of the density-inducing agent (i.e. either salt or heat),  $\kappa$ , to the diffusivity of momentum,  $\nu$ , is expressed by the Schmidt number  $S_c = \nu/\kappa$ . The value of  $S_c$  was 700 and 0.7 for water and wind tunnels respectively.

Sharp density interfaces and stably stratified layers sandwiched between homogeneous layers of different densities occur frequently in the environment; for example, they occur at the base of the oceanic thermocline and at the top of the convective mixed layer of the atmospheric boundary layer. However, the dynamics and turbulent transport within and through such stable interfaces and layers are less well understood than those for linearly stratified fluid columns. To address this shortcoming, we present the results of an experimental study of shear-free decaying grid-generated turbulence on both sides of a sharp stable density interface between two homogeneous layers of differing densities. Experiments were conducted in a salt-stratified water tunnel so that  $S_c = 700$ . Measurements were made of the evolution of the mean density field  $\bar{\rho}$ , and of  $\rho'$ ,  $u'$ ,  $w'$ , the root-mean-square values for the turbulent fluctuation of density, horizontal velocity and vertical velocity, and of  $\rho w$  the vertical mass flux. Vertical mass flux  $\rho w$  in density-stratified flows is important because of its crucial role in the dynamics (see §2).

The broad objective of this paper is to present the results of direct vertical mass flux measurements, as there is an absence of such measurements for this flow configuration in salt-stratified water. First, we describe how flux evolves both vertically across the interface and with distance from the turbulence-generating grid. This helps to understand the detailed structure of transport through sharp density interfaces. Second, we discuss the results of flow visualization to determine the extent to which interfacial convolutions are suppressed by stratification. We also wish to confirm the observation of Jayesh, Yoon & Warhaft (1991) who, from experiments in an identical flow configuration in a thermally stratified wind tunnel ( $S_c = 0.7$ ), found that the growth of the mixed interfacial layer is arrested and reversed when buoyancy forces are dominant. Third, we compare the magnitudes of flux, turbulent potential and kinetic energy between wind and water tunnel experiments to discriminate molecular effects.

After reviewing relevant research in §2, the experimental apparatus and instrumentation are described in §3. Results and discussion are presented in §4, and the conclusions follow in §5.

## 2. Previous work

In this section we review previous studies of decaying grid-generated turbulence under conditions of stable stratification. Stable stratification influences the turbulent field because energy is depleted by work against gravity so that, relative to the otherwise identical passive configuration (i.e. without density stratification), velocity variances may be expected to diminish. That is to say, the relative inertial/buoyancy force balance is central to the understanding of the dynamics. It is most simply expressed by the product of the buoyancy frequency  $N = (-g/\bar{\rho})(\partial\bar{\rho}/\partial z)^{1/2}$  (where  $\bar{\rho}$  is the mean density,  $g$  is the acceleration due to gravity acting in the  $-z$  direction, see figure 1) and turbulent timescale  $t = l_u/u'$  (where  $u'$  and  $l_u$  are the turbulent (integral)

velocity and lengthscales). For decaying grid-generated turbulence (due to the decay of velocity variances), the relative effects of buoyancy forces increase with distance from the grid. Consequently the ratio of the inertial/buoyancy force balance expressed by the turbulent Froude number,  $F_R = u'/Nl_u$ , decreases with distance. Equating the integral lengthscale with the dissipation rate lengthscale,  $l = u'^3/\epsilon$  (e.g. Tennekes & Lumley 1982), results in the corresponding turbulent velocity  $u' = (\epsilon l)^{1/3}$ . Thus it is possible to derive a lengthscale characterizing buoyancy effects by equating buoyancy and inertial forces – the Osmidov scale  $l_o = (\epsilon/N^3)^{1/2}$ ; stratification effects predominate when  $l_o < l_u$ . That the ratio of the lengthscales describes the relative force balance is seen by also noting that  $F_R = (l_o/l_u)^{2/3}$ . Another interpretation of  $F_R = u'/Nl_u$  is in terms of timescales, since  $N$  has dimensions of  $(\text{time})^{-1}$ ; that is,  $F_R = u'/Nl_u = (Nt)^{-1}$  where  $t$  is the turbulent timescale. In other words, if  $F_R$  is large or  $Nt$  is small, the turbulence will be largely unaffected by stratification and so the turbulence will decay in approximately the same manner as the passive case. Buoyancy forces will predominate because the integral lengthscale of the turbulence becomes of the order of (and eventually exceeds) the Osmidov scale.

These lengthscales, however, are useful only in determining if the effects of stratification are likely to be significant for they do not address the interplay between turbulent kinetic energy,  $E_{TK}$ , and turbulent potential energy,  $E_{TP}$ , from whence much of the complexity arises. For example, the decaying grid-generated turbulence experiments to be described below show that mixing converts kinetic energy into potential energy so that kinetic energy in a stratified fluid is less than in a homogeneous fluid. This does not necessarily mean an increased dissipation rate, as the decay rate of the sum of  $E_{TP}$  and  $E_{TK}$  is approximately the same as in the homogeneous case. These findings suggest that the decay of the total energy is determined by a dissipation rate  $\epsilon_{E_{TP}}$  for density fluctuations  $\rho$ , in addition to the usual kinetic energy dissipation rate  $\epsilon$  (Ellison 1957; Townsend 1958). Since the total turbulent energy,  $E$ , comprises  $E_{TK}/\text{unit mass} (= \frac{1}{2}u_i'^2)$  and  $E_{TP}/\text{unit mass} (= -\frac{1}{2}(g/\bar{\rho})(\partial\bar{\rho}/\partial z)^{-1}\bar{\rho}^2)$  it follows that for linearly stratified decaying grid-generated turbulence (Riley 1985)

$$\bar{U} \frac{\partial}{\partial x} (E_{TK}) = -\frac{g}{\bar{\rho}} \overline{\rho w} - \epsilon_{E_{TK}}, \quad (1)$$

$$\bar{U} \frac{\partial}{\partial x} (E_{TP}) = \frac{g}{\bar{\rho}} \overline{\rho w} - \epsilon_{E_{TP}}. \quad (2)$$

Therefore,

$$\bar{U} \frac{\partial}{\partial x} (E) = -(\epsilon_{E_{TK}} + \epsilon_{E_{TP}}), \quad (3)$$

where, as usual,  $\epsilon_{E_{TK}} = \nu(\overline{\partial u_i/\partial x_j})^2$  and  $\epsilon_{E_{TP}} = -\kappa g/\bar{\rho}(\partial\bar{\rho}/\partial z)^{-1}(\overline{\partial\rho/\partial x_j})^2$  and  $\nu$  is the kinematic viscosity, with  $\kappa$  the mass diffusivity and overbars represent time averaging. It is important to appreciate that the buoyancy flux  $((g/\bar{\rho})\overline{\rho w})$  is significant dynamically – by linking the potential and kinetic energy evolution equations in such a way that a gain in potential energy corresponds to a loss in kinetic energy, and vice-versa, so admitting the possibility of wave-like behaviour.

Lagrangian analyses (Csanady 1964; Pearson, Puttock & Hunt 1983) of the vertical diffusion of marked fluid elements in stratified turbulent flows show that the flux of density can be expressed as a sum of the growth of the displacements and molecular mixing between fluid elements. In particular these analyses show that flux is asymptotically proportional to  $w^2$ , so that for increasingly large stratification as

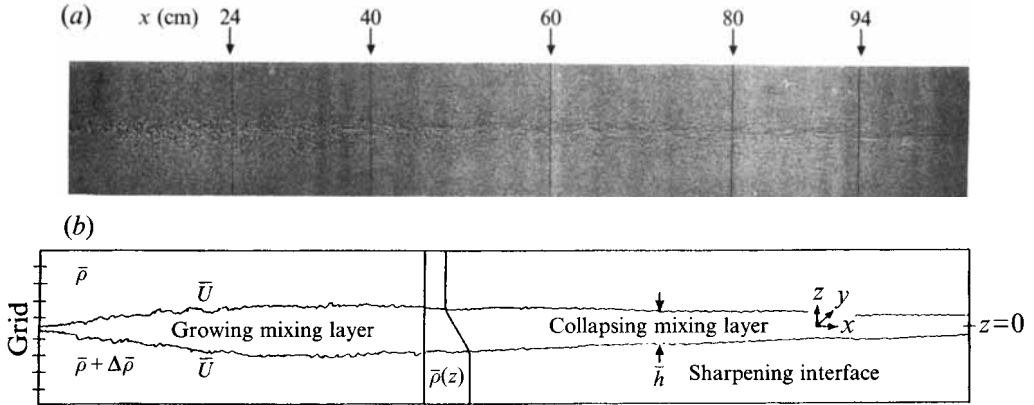


FIGURE 1. (a) Shadowgraph of evolving stratified flow. (Flow is from left to right  $\Delta\bar{\rho} = 3 \text{ kg m}^{-3}$ ,  $R_{iM} = 0.16$ .) (b) Schematic of shadowgraph. Also indicated in a right-handed coordinate system.

vertical motions diminish so does the flux. Furthermore, assuming that densities of fluid elements remain unchanged, there is an 'equivalence between specifying that an element is a distance  $z'$  above its equilibrium level, and specifying that its density is  $\rho'$  greater than the mean' at the equilibrium level for a stable linear gradient (Pearson *et al.* 1983). This leads to a lengthscale  $l_\rho = \rho' / (d\bar{\rho}/dz)$  which is representative of the typical vertical distance travelled by fluid elements before returning to their equilibrium level. A second lengthscale,  $l_B = w'/N$ , is indicative of the average vertical distance travelled by fluid elements in converting *all* their kinetic energy into potential energy.

The decay of (initially) isotropic turbulence in a linearly stratified environment has been studied numerically by Riley, Metcalfe & Weissman (1981) and Metais (1985), and using rapid distortion theory by Stretch (1986). Their results show that the total turbulent energy ( $E_{TK}$  and  $E_{TP}$ ) decayed as  $t^{-B}$  (with  $B \approx 1$ ). No transition in the total decay rate occurred, but it was noted that the vertical kinetic and potential energies were oscillatory, mutually out of phase. The vertical kinetic energy was less than half the horizontal, which indicated that the energy-containing motions were anisotropic. Horizontal velocities were not changed as much as the vertical velocity, the difference between them being a compensating turbulent potential energy so that the total (kinetic and potential) dissipation rate was little affected by stratification. The vertical density flux was observed to diminish to zero at  $Nt \sim \frac{1}{2}\pi$ , and then to oscillate with significant counter-gradient flux until  $Nt \sim 2\pi$  when the flux was negligible.

For a two-layer density stratification, the ratio of buoyancy to inertial forces can be expressed by the Richardson number  $R_i = g' l_u / u'^2$ , where  $l_u$  is the integral length derived from autocorrelation of the fluctuating  $u$ -signal of the turbulent velocity field,  $u'^2$  is the variance of the fluctuating velocity  $u$ , and  $g'$  is the reduced gravitational acceleration  $g' = g \Delta\bar{\rho} / \bar{\rho}$  with  $\Delta\bar{\rho}$  the density difference between the two layers. The flow configuration of a two-layer density stratification in the present experiment differs from a linear density gradient profile in that the density gradient is vertically inhomogeneous. Relative to the linear density gradient profile, there are additional contributions to transport due to vertical divergences associated with the density gradient inhomogeneity. From experiments with an identical flow configuration to the present study, but undertaken in a thermally stratified wind tunnel (i.e.  $S_c = 0.7$ ), Jayesh *et al.* (1991) found that the effect of the transport from the additional divergences, principally  $(\partial/\partial z)(\bar{\rho}w)$ ,  $(\partial/\partial z)(\frac{1}{2}\bar{\rho}^2w)$  and  $(\partial/\partial z)(\overline{w^2\rho})$  – the vertical gradients of the

buoyancy flux, the transport of buoyancy flux and the transport of temperature variance – did not have a profound effect. That is, they found that decaying grid-generated turbulence in a two-layer stratification evolved in a similar manner to decaying grid-generated turbulence in a linearly stratified fluid column. Jayesh *et al.* (1991) also found that a mixed layer formed at the interface between the homogeneous layers of differing densities. Their measurements showed that this interfacial mixed layer possessed a linear density gradient, and that the value of this mixed layer linear density gradient was constant for all distances downstream of the turbulence-generating grid. Jayesh *et al.* (1991) concluded that the effects of the density gradient inhomogeneity and vertical divergences were small: for decaying grid-generated turbulence ‘the rapid decay of the velocity variance, with concomitant increase in buoyancy effects, dominates over the effects of transport’ (Jayesh *et al.* 1991).

### 3. Experimental set-up and apparatus

A recirculating two-layer stratified water tunnel was designed and built for the experiments. The tunnel was 15 cm wide, 20 cm deep and 225 cm long, and was constructed from 1.27 cm thick Plexiglas. Details of the water tunnel and related apparatus are given in Huq (1990). Figure 1 shows the flow configuration comprising two layers of uniform but different densities that result in a stably stratified, two layer shear-free flow. Each layer was driven from a storage reservoir by a centrifugal pump.

The density difference between the layers was generated by adding brine ( $S_c = 700$ ) to the storage reservoir of the lower layer. Coarse and fine mesh screens, which were located upstream of the turbulence-generating grid, reduced the background turbulence to  $w'/\bar{U} = 0.2\%$ . Mean velocities of the upper and lower layers were identical in value, and little interfacial mixing was observed in the ambient flow. The turbulence generating-grid comprised bars of width  $d = 0.64$  cm, and thickness  $s = 0.2$  cm, arranged in a square mesh with spacing  $M = 3.2$  cm between bars. The mean velocity  $\bar{U}$  of the layer was kept constant throughout the experiments at a value of  $\bar{U} = 7.7$  cm s<sup>-1</sup>. Thus the parameters based on the grid dimensions were the mesh Reynolds number  $R_M = \bar{U}M/\nu \approx 2500$ , the grid spacing to bar size ratio  $M/d = 5$ , and the grid solidity = 36%.

Salinity measurements were determined by using an aspirating conductivity probe with a 1 mm diameter sensor of 2 mm length and an end orifice of 0.33 mm. The aspirating conductivity probe was operated in an AC bridge operating at 2 KHz. The frequency response and spatial resolution of the aspirating conductivity probe were estimated from plunge tests through a sharp density interface to be 70 Hz and 0.4 mm respectively.

Two components ( $u, w$ ) of the velocity field were measured using quartz-coated TSI cylindrical X-films (Type 1241-60w) of dimensions 0.15 mm diameter and 2.03 mm length. The X-films were driven by a PSI Model 6100 anemometer operated with 4% overheat in the constant-temperature mode. As the temperature of the fluid of the recirculating stratified water tunnel increased by only 0.2 °C/hour from frictional heating, and as the typical duration of an experiment was half an hour, it was not necessary to employ temperature correction procedures for the X-films. However, to account for the small length to diameter ratio ( $\sim 15$  for the TSI 1241-60w hot films) yaw corrections with  $k = 0.25$  were applied (Champagne & Sleicher 1967; Lawson & Britter 1983).

Flux measurements were obtained by correlating the signals of the aspirating conductivity probe and the X-films, which were located 1 mm from each other. The

spatial resolution of the ‘flux probe’ (i.e. the combined aspirating conductivity and X-film probes) was estimated to be 1.5 mm. The signals were subsequently digitized at 50 Hz by a 12-bit A–D interface and stored on flexible disks. Statistical analyses of the digitized data were obtained by standard software: spectral analysis was done by a HP54410/54203 signal analyser. Typical values of the errors of root-mean-square values of velocity and density fluctuations, and their correlation measurements, were 5% and 10% respectively.

A 1 mm thick light sheet, produced by using sodium fluorescein dye and a water-cooled argon-ion laser (Lexcel Model 95, operating at 2 W), as well as shadowgraphs, were used to visualize the flow. Experiments were performed using salt as the buoyancy-inducing agent in a water tunnel (i.e.  $S_c = 700$ ). The density difference between the layers was varied so that the range of Richardson number  $R_i = ((\Delta\bar{\rho}/\bar{\rho})g)l_w/u'^2$  for the experiments was  $0 < R_i < 110$ . In terms of the parameter  $Nt$ , the product of the buoyancy and turbulent timescales  $N$  and  $l/u'$  respectively, the range of values covered in the experiments was  $0 < Nt < 15$ . Values of the mesh Richardson number  $R_{iM} = ((\Delta\bar{\rho}/\bar{\rho})g)M/\bar{U}^2$  for the experiments varied between  $0.02 < R_{iM} < 0.16$ .

#### 4. Results and discussion

The results from flow visualization are discussed in §4.1. Quantitative results of the measurements of the density, velocity and flux fields follow. In §4.2, measurements of the mean density profiles show how the sharp interface is perturbed by the grid-generated turbulence to form a mixed layer. While this mixed layer initially grows, it becomes subsequently very thin. Details of the evolution of the turbulent velocities ( $u'$ ,  $w'$ ) are presented in §4.3. Measurements revealed that values of both  $u'$  and  $w'$  in the mixed layer were different from values far from the mixed layer. The measurements of density fluctuation of §4.4 established that the magnitudes of density fluctuation attenuate with increasing density difference (i.e. with  $R_i$  or  $Nt$ ). One effect of density stratification is that buoyancy flux is inhibited, and this is quantified in §4.5. Finally, the dependence of entrainment rates and mixing efficiencies on density stratification are described in §4.6.

##### 4.1. Flow visualization

A shadowgraph of the developing interfacial region (figure 1,  $\Delta\bar{\rho} = 3 \text{ kg m}^{-3}$ ,  $R_{iM} = 0.16$ ) shows that the growth of the mixed region reaches a maximum at 30 cm. Later measurements show that this is approximately the location where  $\overline{\rho w} \approx 0$  and where  $\rho'$  reaches a maximum. Thereafter (i.e.  $x > 40$  cm) there is an increasingly striated appearance, and simultaneously the mixing layer thickness (indicated by the extent of density fluctuations which give rise to the observed refractive index variations) was seen to collapse gradually so that the mean interface sharpened. At  $x = 94$  cm several nearly uniform horizontal striations, each of order 1 mm in vertical scale, constituted the interface. The uniformity of appearance at  $x = 94$  cm suggests that mixing events (which reduce the uniformity of appearance) are rare in comparison to regions further upstream.

The LIF visualization of figure 2 shows the instantaneous interface to be sharp. Unlike the passive or zero-density-difference (i.e.  $R_i = 0$ ) interface of billow- and wedge-like convolutions and large displacements from the mean (see figure 2*a* of Huq & Britter 1995), the present large  $R_i$  interfaces are more quiescent. Billows and wedges are less common, and generally there are fewer features; broadly, ‘events’ are rarer and smaller in volume than for the  $R_i = 0$  case. Visualizations, such as figure 2, were analysed to determine displacements of the dyed fluorescein from the location of the

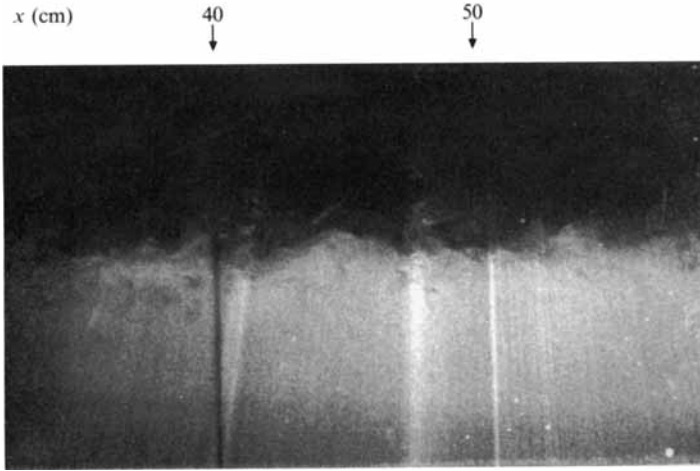


FIGURE 2. Longitudinal section from LIF ( $x, z$ -plane). (Flow is from left to right,  $\Delta\bar{\rho} = 3 \text{ kg m}^{-3}$ ,  $R_{iM} = 0.16$ ,  $S_o = 700$ .)

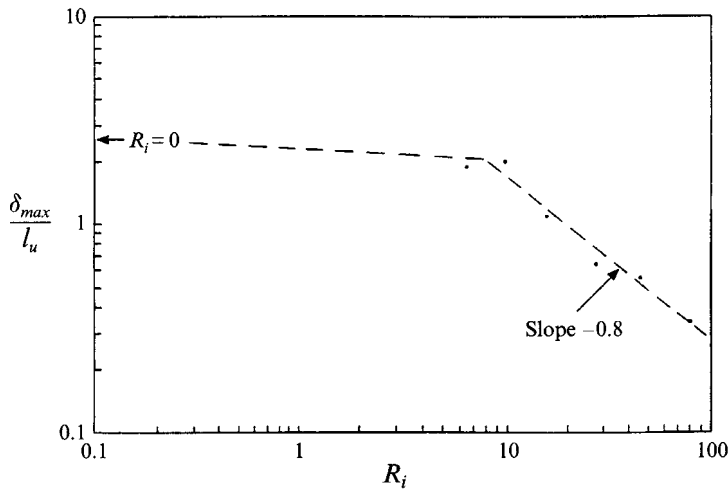


FIGURE 3. Influence of Richardson number  $R_i$  on maximum interfacial displacement  $\delta$ . Ordinate is non-dimensionalized by the integral lengthscale  $l_u$  determined from autocorrelation of the  $u$ -velocity signal  $l_u = l_{R_{11}}(r, 0, 0)$  from passive case. Slope of  $-0.8$  is a best fit line.

mean interface (which is defined as  $z = 0$ ). Typically, maximum displacements were the average of the peak value obtained from each of five photographs. The results presented in figure 3 show that the extent of the maximum observed interfacial displacement,  $\delta$ , from the mean interface is reduced by stratification. It is evident that the effects of stratification are stronger for  $R_i > 10$ . In figure 3,  $l_u$  is the longitudinal integral lengthscale (determined from the autocorrelation of the fluctuating  $u$ -signal in the passive, i.e. unstratified case). Note that a  $\delta_{max}/l_u \sim R_i^{-1}$  variation arises if we consider a balance between vertical kinetic energy and the work done against buoyancy forces, i.e.  $\delta \sim w'^2/g'$ . The observed slope of  $-\frac{4}{5}$  is close to  $-1$  which suggests significant internal wave activity for  $R_i \geq 10$ .

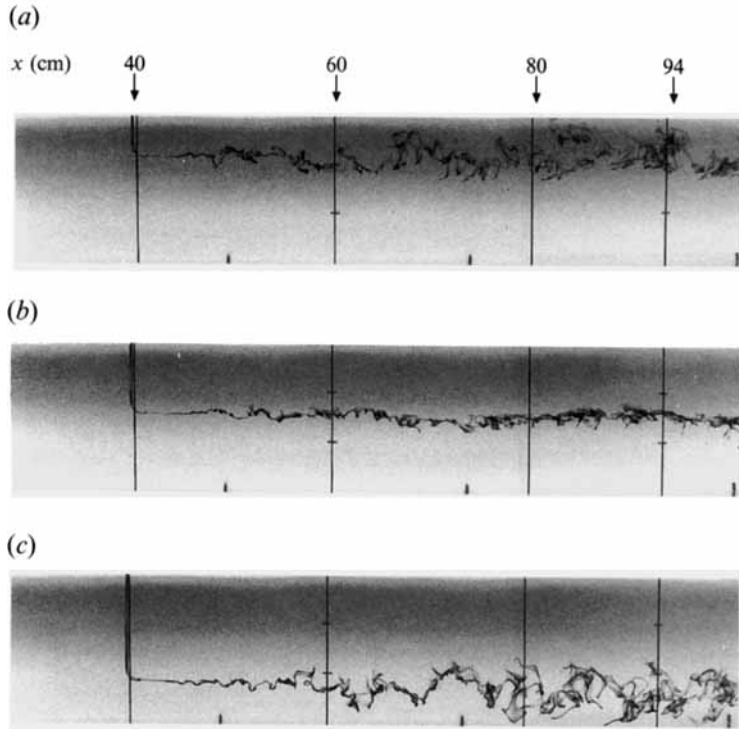


FIGURE 4. Attenuation of vertical motions by stratification. ( $\Delta\bar{\rho} = 3 \text{ kg m}^{-3}$ ,  $R_{iM} = 0.16$ .) Vertical displacements of dye released at centre of interface are small. Dye released (a) above interface, (b) at interface, (c) below interface.

The attenuation of vertical motions by stratification is also shown vividly by figure 4. On either side of the interface, turbulence from the grid causes the line of released dye to become convoluted and space-filling. At the interface, the region of strongest density gradients, the vertical growth is seen to be severely inhibited. Note that the horizontal growth was observed to be similar to that away from the interface, and similar to the unstratified case.

#### 4.2. Mean density profiles

Downstream of the grid the mean density profiles (figure 5a) have a linear gradient near the centreline with well mixed layers away from the centreline so that  $d\bar{\rho}/dz$  is a maximum at the centre of the interface (figure 5c). The relative change in mean density profile between longitudinal sections of figure 5(a) (and shown explicitly in figure 5b for  $x = 0$  and 24 cm) indicates the presence of a vertical mass flux. The very much smaller difference between the profiles at  $x = 24$  cm and  $x = 94$  cm (of figure 5a) imply reduced mass flux, a finding consistent with the flow visualizations. The departure from the passive evolution is shown clearly in figure 6 which shows the rate of growth of the half-width,  $\bar{h}$ , determined by the intercept of the extrapolation of the central linear density gradient to the vertical ordinate axis, i.e.  $\Delta\bar{\rho}/(d\bar{\rho}/dz)_{z=0}$ . Initially the growth is similar to that of the passive case, but  $\bar{h}$  attains a maximum value and diminishes thereafter as buoyancy forces predominate (e.g. for  $\Delta\bar{\rho} = 0.5 \text{ kg m}^{-3}$ , the maximum value of  $\bar{h}$  occurs at  $x = 40$  cm).

The buoyancy frequency,  $N$ , at the centre of the interface, was found to remain



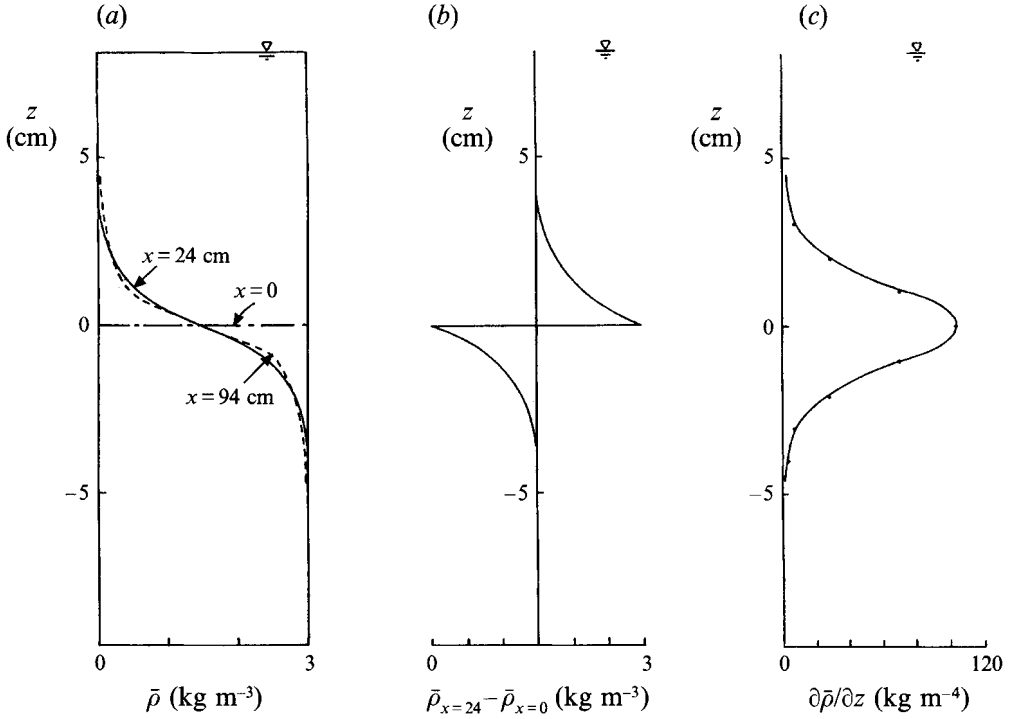


FIGURE 5. Mean density profiles for  $\Delta\bar{\rho} = 3 \text{ kg m}^{-3}$ : (a) Mean density profiles,  $R_{iM} = 0.16$  at  $x = 0, 24$  and  $94$  cm. (b) Relative change in mean density profiles between  $x = 0$  and  $24$  cm. (c) Mean density gradient profile at  $x = 24$  cm for showing a maximum at the centre of the interface.

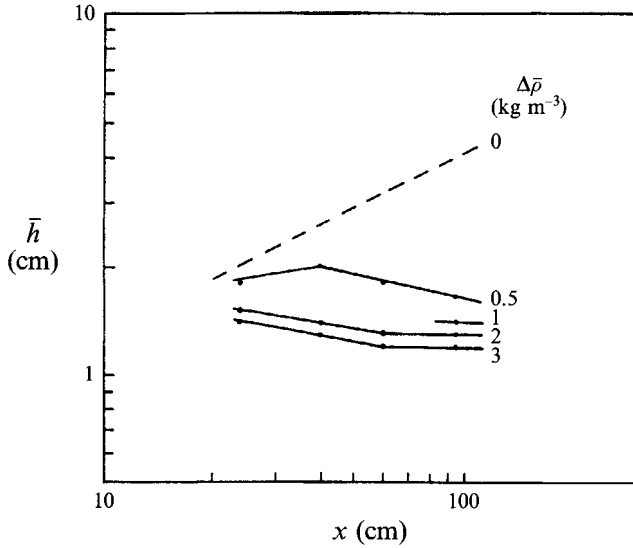


FIGURE 6. Evolution of mean interface half-width  $\bar{h}$ . Dashed line is best fit line of passive case data (i.e.  $\Delta\bar{\rho} = 0$ ). Values of  $R_{iM}$  for  $\Delta\bar{\rho} = 0.5, 1, 2, 3 \text{ kg m}^{-3}$  are 0.03, 0.05, 0.11 and 0.16 respectively.

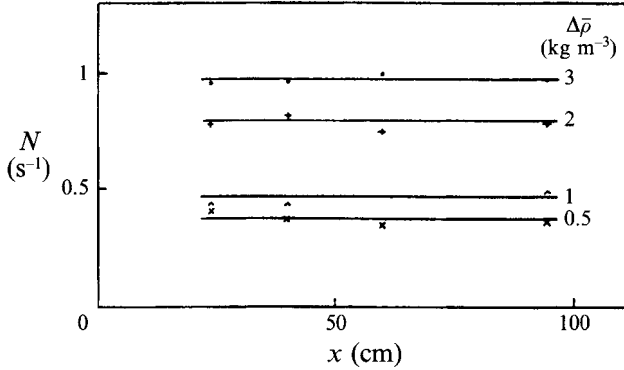


FIGURE 7. Buoyancy frequency  $N$  at centre of mean interface,  $z = 0$ .

constant downstream for a given density difference (figure 7). This facilitates comparison of the timescales of the turbulence  $t$  and the buoyancy timescale  $N^{-1}$ , despite this not being a uniformly stratified fluid column. Owing to the decay of velocity variances the timescales ratio  $Nt$  increases with distance from the grid (figure 8a). The turbulent timescale  $t$  in figure 8(a) was taken to be equal to the advection time  $x/\bar{U}$  which is known to be valid for decaying grid-generated turbulence (Tennekes & Lumley 1982). (It should be noted that over the length of the water tunnel that the timescale  $l_u/u'$  was approximately equal to 2/3 of the value of the advection time  $x/\bar{U}$  from the grid.) For the present two-layer stratification the buoyancy timescale is determined by the extent of the buoyancy jump, namely  $(g'/2\bar{h})^{-1/2}$ . It was found during the course of the experiments that  $(g'/2\bar{h})^{1/2} t = Nt$  to within 10%. Consequently, subsequent comparison of the timescales is expressed in terms of  $Nt$ . The equivalence between the two-layer and wholly linearly stratified profile at the centre of the interface can be illustrated by noting that  $R_i = g'l_u/u'^2$  is the square of the ratio of the eddy and buoyancy timescales,  $l_u/u'$  and  $(g'/l_u)^{-1/2}$  respectively, so that  $R_i \sim (Nt)^2$ . This is demonstrated to be the case in figure 8.

#### 4.3. Velocity field

In this section, the evolution of turbulent velocities for the stratified case are discussed and compared with values in the absence of stratification (i.e.  $\Delta\bar{\rho} = 0$ ). Figure 9(a, b) indicates that the effect of stratification is to attenuate the velocity variances. The turbulent kinetic energy ( $E_{TK}$ ) assumed to be  $\frac{1}{2}q^2 = \frac{1}{2}(2u'^2 + w'^2)$  as the  $v$ -component was not measured, has a similar decay behaviour for both passive and stratified cases. For the passive case, the decay curves are of the form  $(u'_i/\bar{U}) = A(x/M - 4)^{-1.4}$  with  $A = 0.07, 0.05$  for  $u', w'$  respectively. These decay curves agree with reported grid-turbulence data (e.g. Sreenivasan *et al.* 1980). The reduction in  $w'^2$  is proportional to the density difference for  $x < 60$  cm; for  $x > 60$  cm there is a reduction in the decay rate (increasing with density difference), see figure 9(b). Changes in the values of  $u'^2$  are less marked, with values of  $u'^2$  for  $\Delta\bar{\rho} = 3 \text{ kg m}^{-3}$ ,  $R_{iM} = 0.16$  being approximately the same as passive values.

Thomas & Hancock (1977), in their study of grid turbulence near a moving wall with zero mean shear, found that the normal fluctuating velocity component was inhibited and the longitudinal component was amplified within a layer of thickness of  $O(l_u)$  from the moving wall (where  $l_u$  is the longitudinal integral lengthscale of the turbulence well away from the moving wall). For the present zero mean shear density interfaces, the departure from the passive case (i.e.  $\Delta\bar{\rho} = 0$ ) values of  $u'$  and  $w'$  are similar to those of

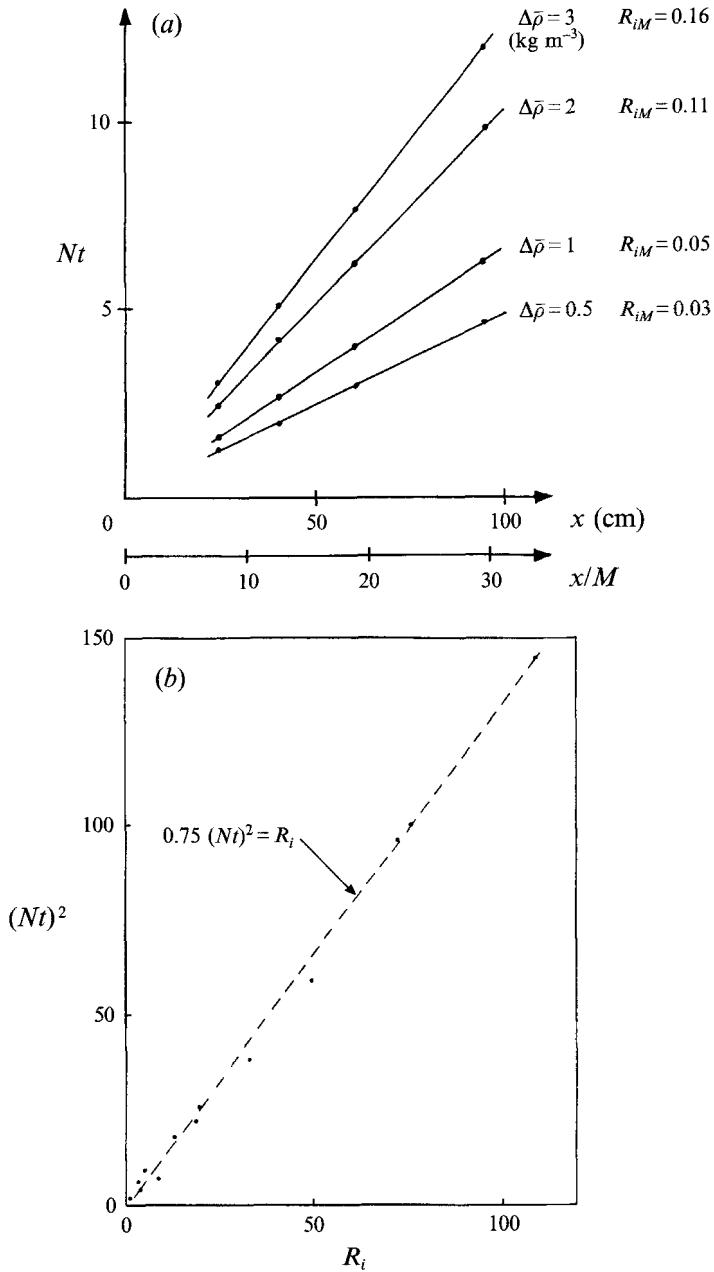


FIGURE 8. (a) The evolution of the parameter  $Nt$  with distance  $x$  from the grid. Note dimensional and non-dimensional abscissa. Also indicated is the mesh Richardson number  $R_{iM}$  for each value of  $\Delta\bar{\rho}$ . (b) Linear relationship between  $R_i$  and  $(Nt)^2$  showing equivalence of  $Nt$  and  $(g'/2\bar{h})^{1/2}t$  scaling at centre of mean interface,  $z = 0$ .

the rigid moving wall of Thomas & Hancock. Figure 10 shows the vertical distributions of  $u'/u'_p$  and  $w'/w'_p$ . The vertical component increased monotonically away from the interface. Also, the value of the ratio at the centre of the interface is seen to decrease with increasing stratification. For the case of the stronger stratification (figure 10b)  $w'$  is attenuated to 70% of the value of the passive case. Similar attenuations of  $w'$  were

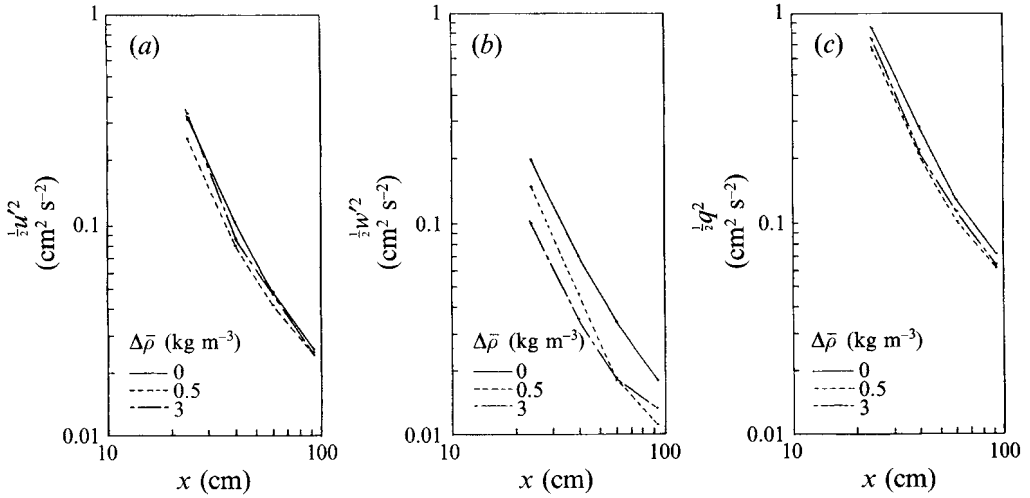


FIGURE 9 (a-c). Decay of turbulent velocity fluctuations at centre of mean interface,  $z = 0$ . Note in (c)  $q^2$  is defined as  $(2u'^2 + w'^2)$  as  $v'$  is not measured.

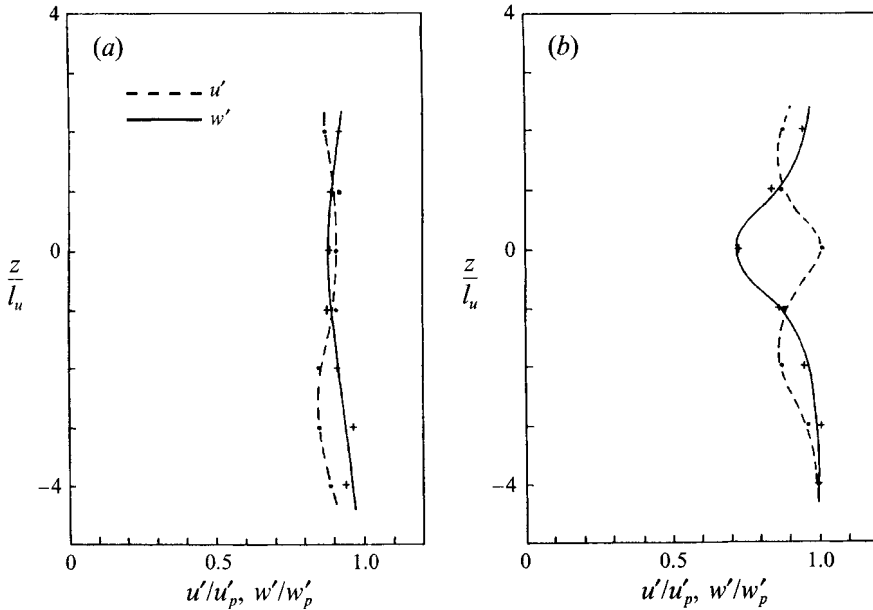


FIGURE 10. Vertical distribution of velocity fluctuations at  $x = 24$  cm. Ordinate is non-dimensionalized by the integral lengthscale  $l_u$ ; abscissa is non-dimensionalized by root-mean-square values of  $u, w$  from the passive case (i.e.  $\Delta\bar{\rho} = 0$ ). (a)  $\Delta\bar{\rho} = 0.5$  kg m $^{-3}$ ,  $Nt = 1.3$ . (b)  $\Delta\bar{\rho} = 3$  kg m $^{-3}$ ,  $Nt = 3.1$ .

found by Jayesh *et al.* (1991). However, the  $u'$ -distribution can be non-monotonic. The increase of  $u'$  for  $z/l_u < 1$  for the more strongly stratified case of figure 10(b) is consistent with the amplification of the lateral velocity components due to distortion of eddies (i.e. 'flattening') by interaction with the flapping instantaneous density interface. Such amplification of  $u'$  can result in  $u'$  being greater than passive values at the centre of the interface. The distributions are symmetrical; and for  $\Delta\bar{\rho} = 3$  kg m $^{-3}$

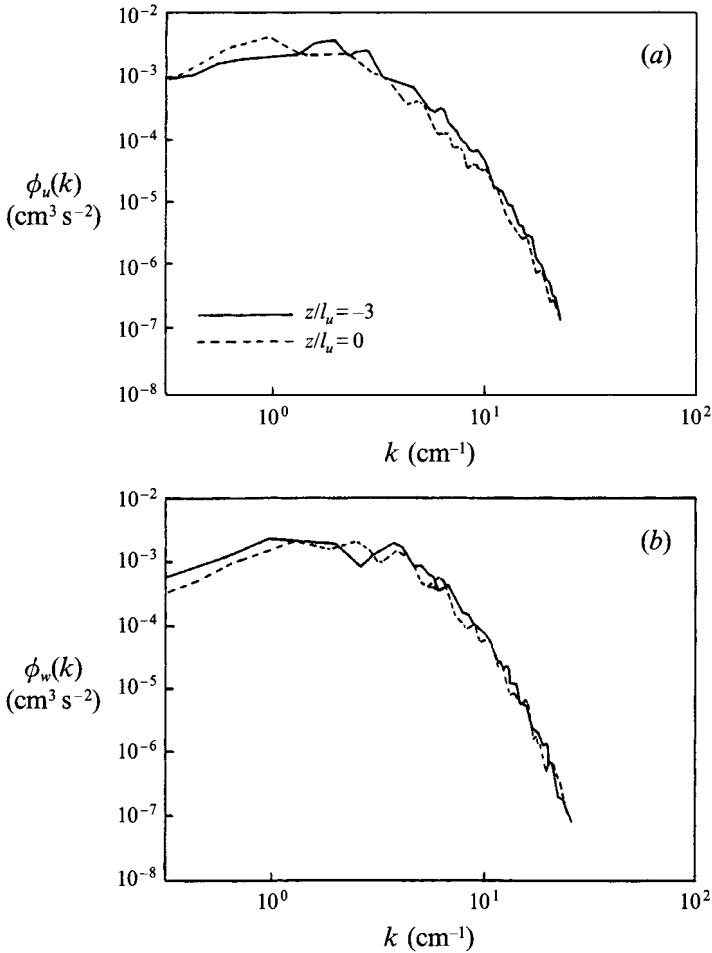


FIGURE 11. One-dimensional spectra ( $\phi_u$  and  $\phi_w$ ). Data for  $\Delta\bar{\rho} = 3 \text{ kg m}^{-3}$  at  $x = 24 \text{ cm}$ ,  $R_{iM} = 0.16$  at centre of interface ( $z/l_u = 0$ ) and away from centre of interface ( $z/l_u = -3$ ).

at  $x = 24 \text{ cm}$  ( $Nt = 3.1$ ), at the centre of the interface  $u'/w' \approx 1.4$ , the minimum of  $u'$  occurs at  $z/l_u \approx 1.5$ . Similar changes in  $u'$  and  $w'$  were also observed for density interfaces in zero mean flow turbulence (i.e. mixing boxes) by McDougall (1979) and Hannoun, Fernando & List (1988) and calculated theoretically by Carruthers & Hunt (1986). Comparison of the spectra of  $u$ ,  $w$  at  $x = 24 \text{ cm}$  ( $\Delta\bar{\rho} = 3 \text{ kg m}^{-3}$ ,  $Nt = 3.1$ ) at the centre of the interface ( $z/l_u = 0$ ) with  $z/l_u = -3$  indicates distortion of the turbulence field (figure 11). The spectral density of the large scales of the  $u$ -component is greater at the centre of the interface, whereas the  $w$ -component is smaller, indicating anisotropy.

The distribution of  $E_{TK}$  is also changed by the stratification. Figure 12 shows the ratio of the  $E_{TK}$  of stratified and passive cases ( $q^2/q_p^2$ ). Clearly the variation is strongly non-monotonic for the strongly stratified case of  $\Delta\bar{\rho} = 3 \text{ kg m}^{-3}$ ,  $R_{iM} = 0.16$ . This is so both for cases with and without a density flux. For the weakly stratified case ( $\Delta\bar{\rho} = 0.5 \text{ kg m}^{-3}$ ,  $R_{iM} = 0.03$ ) the ratio of  $q^2/q_p^2$  is approximately constant ( $\sim 0.8$ ) through the mixed region up to  $z/l_u \sim 5$ . In contrast, values of  $q^2/q_p^2$  return to unity for the strongly stratified case by  $z/l_u \sim 3$ . The implication is that the extent of the region of energy loss from the velocity field is greater for the weakly stratified case. The sum of

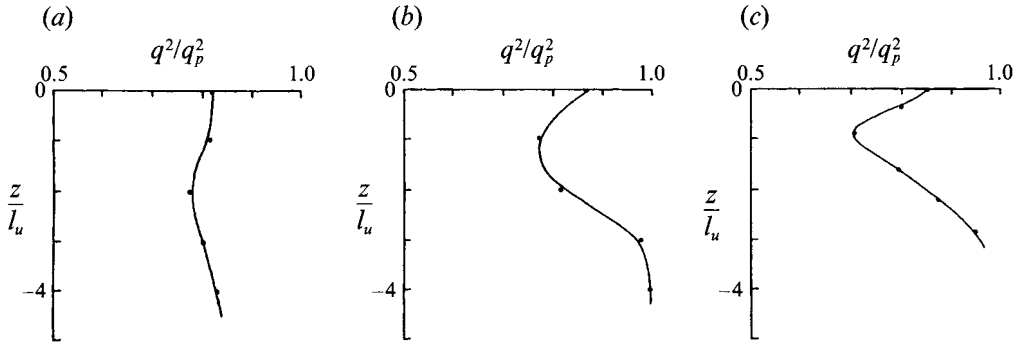


FIGURE 12. Comparison of vertical distribution of turbulent kinetic energy through interface with passive case. Abscissa is non-dimensionalized by  $q_p^2$ , values of the turbulent kinetic energy of the passive case ( $\Delta\bar{\rho} = 0$ ). Ordinate is non-dimensionalized by the integral lengthscale  $l_u$ . Dimensional values of  $l_u$  at  $x = 24$  cm, 60 cm are 1.0 cm and 1.6 cm respectively. (a)  $\Delta\bar{\rho} = 0.5$  kg m $^{-3}$ ,  $x = 24$  cm,  $F = 0.4$ ,  $Nt = 1.3$ ; (b)  $\Delta\bar{\rho} = 3$  kg m $^{-3}$ ,  $x = 24$  cm,  $F = 0.2$ ,  $Nt = 3.1$ ; (c)  $\Delta\bar{\rho} = 3$  kg m $^{-3}$ ,  $x = 60$  cm,  $F = 0$ ,  $Nt = 7.7$ .

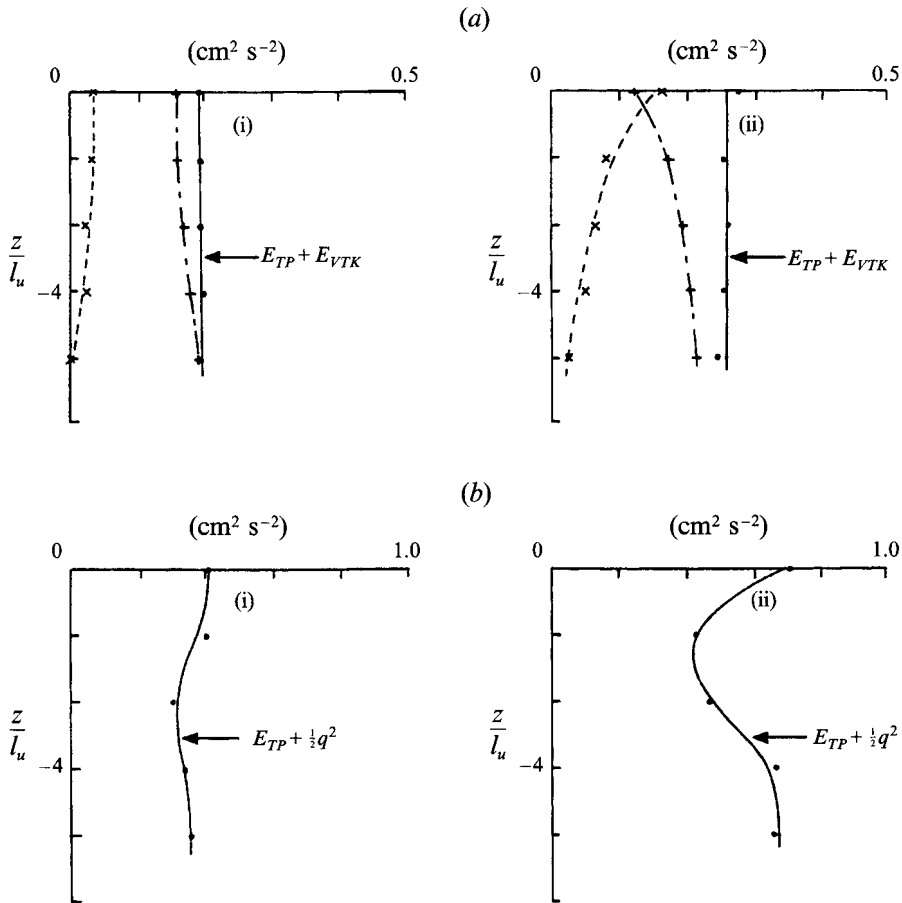


FIGURE 13. Vertical distribution of sum of turbulent potential and kinetic energies at  $x = 24$  cm. (a) Sum of turbulent potential ( $\times$ ) and vertical kinetic energy ( $+$ ). (b) Sum of turbulent potential and kinetic energy. Ordinate is non-dimensionalized by the integral lengthscale  $l_u$ . (i)  $\Delta\bar{\rho} = 0.5$  kg m $^{-3}$ ,  $Nt = 1.3$ ; (ii)  $\Delta\bar{\rho} = 3$  kg m $^{-3}$ ,  $Nt = 3.1$ .

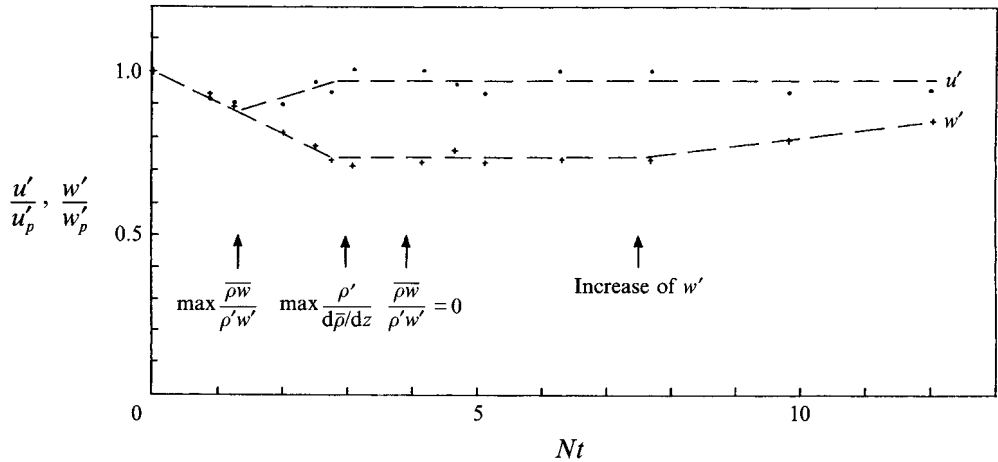


FIGURE 14. Comparison of passive and stratified velocity fluctuations at centre of mean interface,  $z=0$ . Ordinate is non-dimensionalized by root-mean-square values of  $u, w$  of the passive case ( $\Delta\bar{\rho}=0$ ).

the vertical turbulent kinetic energy,  $E_{VTk} = \frac{1}{2}w'^2$ , and turbulent potential energy, defined as  $E_{TP} = (-\frac{1}{2}(g/\bar{\rho})(\rho'^2/(\partial\bar{\rho}/\partial z)))$  for a region of uniform  $N$  (Riley 1985), is found to be constant through the interface up to  $z/l \sim 5$  for both  $Nt = 1.3$  and  $Nt = 3.1$  (figure 13a). Though this suggests partitioning of energy between  $E_{VTk}$  and  $E_{TP}$ , the result is perhaps fortuitous for the sum of the turbulent kinetic energy and turbulent potential energy (i.e.  $E_{TK} + E_{TP}$ ) is found to be non-monotonic, particularly for  $Nt = 3.1$  (figure 13b). Note that for a region of non-uniform  $N(z)$  the definition of  $E_{TP}$  should include a series of terms involving the rate of change of  $\rho'$  with  $z$  (Holliday & McIntyre 1981). The above definition of  $E_{TP}$  is a first-order estimate for a flow with varying  $N$ . Thus it should be understood that the calculated values of  $E_{TP}$ , of figure 13, were approximate for distances greater than  $z/l_u > 1.8$  for  $Nt = 1.3$  and  $z/l_u > 1.4$  for  $Nt = 3.1$  (which were beyond the extent of the region of linear density gradient in the mixed layer). The significance of the stationary point of  $q^2/q_p^2$  and  $(E_{TP} + \frac{1}{2}q^2)$  at  $z/l_u \approx 1$  for the strongly stratified case is that it marks the position where the energy flux changes sign. That the energy flux may change sign on either side of the stationary point suggests that energy may be trapped within a central layer bounded by  $z/l_u = \pm 1$ . So this region acts as a 'wave-guide' (Turner 1973). The data indicate that the lateral dimension of the wave-guide is of  $O(l_u)$ .

The evolution of the velocity field for decaying grid-generated turbulence is described traditionally in terms of the decay of  $u_i'^2$  with  $x/M$ , as in figure 9. However, comparison of the *ratio* of turbulent velocities from the passive and stratified cases (i.e.  $u'/u'_p$  and  $w'/w'_p$ ) is more revealing. Referring to figure 14, in the absence of stratification (i.e.  $Nt = 0$ ),  $u'/u'_p = w'/w'_p = 1$  for all times. For  $Nt < 1$  buoyancy forces are not yet important, and there are significant rates of mixing driven by the turbulent velocity field so that *both*  $u', w'$  diminish in comparison to the passive case values; the minimum ratio coincides with the maximum values of flux. For  $Nt > 1$ , buoyancy effects are increasingly important (and the flux diminishes, see §4.5). But  $u'$  values recover to near passive values, with  $w'$  being inhibited by stratification to near constant values of 70% of the passive values till  $Nt \sim 7.5$  when  $w'$  also recovers. It is not yet understood why there is a transition in the evolution of the velocity field at  $Nt \sim 7.5$ . We remark that the lengthscale  $l_B = w'/N$  exceeds the Osmidov scale  $l_O = (\epsilon/N^3)^{1/2}$  at

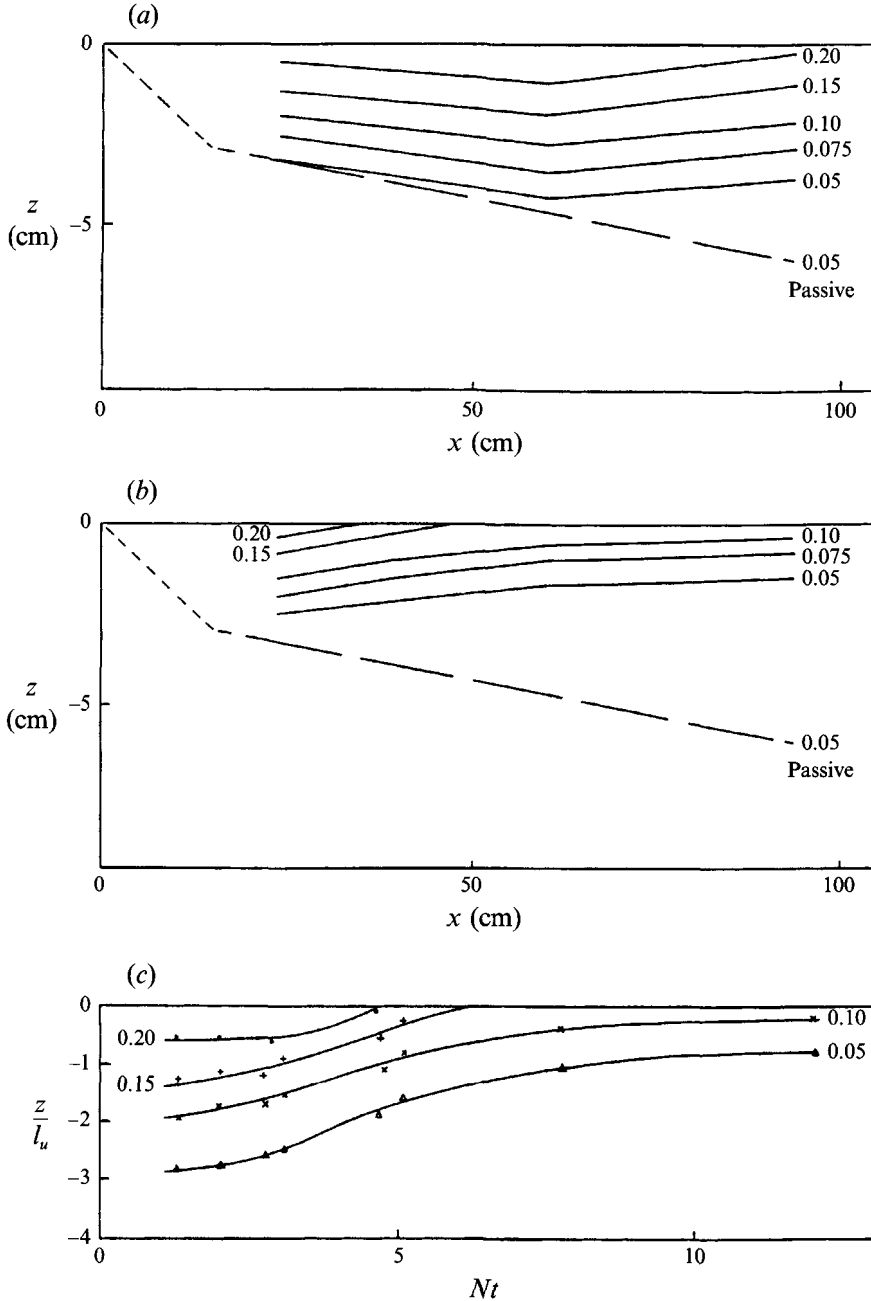


FIGURE 15. Evolution of density fluctuations  $\rho'/\Delta\bar{\rho}$ . (a) Small density difference  $\Delta\bar{\rho} = 0.5 \text{ kg m}^{-3}$ ,  $R_{iM} = 0.03$ . (b) Large density difference  $\Delta\bar{\rho} = 3 \text{ kg m}^{-3}$ ,  $R_{iM} = 0.16$ . (c) Non-dimensionalized plot of evolution of density fluctuations. Schmidt number  $S_c = 700$ .

$Nt = 7.5$  (see figure 18). The dissipation rate  $\epsilon$  in the determination of  $l_o$  is taken from passive case values given by  $\epsilon = 0.147 (\bar{U}^3/M)(x/M-4)^{-2.4}$ . Owing to the vertical inhomogeneity of the velocity field of the stratified flow, it is difficult to evaluate the dissipation rate  $\epsilon$ . In wind tunnel experiments with a linear density gradient Lienhard & Van Atta (1990) and Yoon & Warhaft (1990) found that the dissipation rate  $\epsilon$  is not



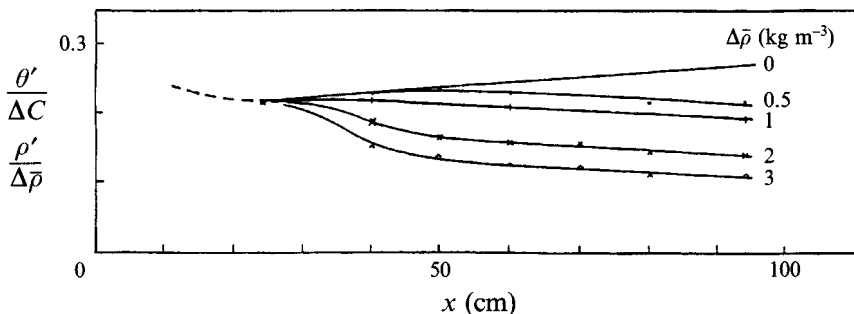


FIGURE 16. Evolution of density fluctuations at centre of mean interface,  $z = 0$ . Data for various values of  $\Delta\bar{\rho}$ .  $S_c = 700$ .

strongly affected by the level of stratification. Their method of calculating  $\epsilon$  was based on assumptions of isotropy, assumptions which may not be valid in a stratified flow. Clearly, further work on the effect of stratification on  $\epsilon$  is desirable. For present purposes the similar forms of the decay of the turbulent kinetic energy  $\frac{1}{2}q^2$  of figure 9(c) for the passive and stratified cases suggest similar dissipation rates.

#### 4.4. Density fluctuations

The evolution of density fluctuations ( $S_c = 700$ ) differs markedly from passive scalar fluctuations as the growth of fluctuations is arrested at large downstream distances from the grid where buoyancy forces become important (figure 15a). For the strongly stratified case (figure 15b), the evolution is a gradual decrease in the intensity of fluctuations from peak values close to the grid. Comparison of  $\rho'/\Delta\bar{\rho}$  contours in terms of  $Nt$  scaling (figure 15c) shows a sharply collapsing flow field for  $2.5 < Nt < 6$  with an altogether more gradual diminution for  $Nt > 7$ . Indeed the nearly horizontal contours away from the interface centreline ( $z/l_u = 0$ ) for  $Nt > 7$  suggest a slowly changing interface with little dissipation of density fluctuations (i.e.  $\kappa(\partial\rho/\partial x_k)^2 \approx 0$ ). This may also be inferred from visual inspection of the shadowgraph in figure 1.

As for the passive case, the maximum fluctuations occur at the centre of the interface; however, stratification reduces the intensities, with reduction occurring earlier for larger density differences (figure 16). This is reinterpreted in terms of the lengthscale  $l_\rho (= \rho'/(d\bar{\rho}/dz))$  in figure 17. Recall that  $l_\rho$  is representative of the typical vertical displacement of fluid elements from their equilibrium level, as opposed to  $l_B = w'/N$  which is the typical vertical distance which could be travelled by a fluid element in converting *all* its vertical kinetic energy into potential energy. It is evident that stable stratification inhibits the lengthscale  $l_\rho$ . Figure 18 is a collation of three lengthscales ( $l_\rho$ ,  $l_B$  and the Osmidov scale  $l_o$ ) at the centre of the interface. For this developing flow configuration, the Osmidov scale  $l_o$  evolved as  $(Nt)^B$  with  $B \approx -1$ . This is in agreement with dimensional arguments  $\epsilon \sim -(d/dt)(\frac{1}{2}q^2) \sim t^{-2}$  for decaying grid-generated turbulence (Tennekes & Lumley 1982); thus  $l_o = (\epsilon/N^3)^{1/2}$  varies as  $t^{-1}$ . In the present study  $l_B$  is found to evolve similarly until the location of the occurrence of the maximum density fluctuation (at  $Nt \approx 3$ ). Thereafter a more gradual evolution ensued as  $(Nt)^{-3/4}$ . Eventually  $l_B$  exceeds  $l_o$  (so that buoyancy effects dominate inertial effects) at  $Nt \approx 7.5$ .  $Nt \sim 7.5$  coincides with a transition in the evolution of the vertical velocity field (see figure 14). Indicated on figure 18 are the locations of maxima of  $\bar{\rho}w/\rho'w' = F$  (from flux measurements of §4.5),  $l_\rho$ , and the location of  $F = 0$ . These results, in conjunction with flow visualization, indicate that

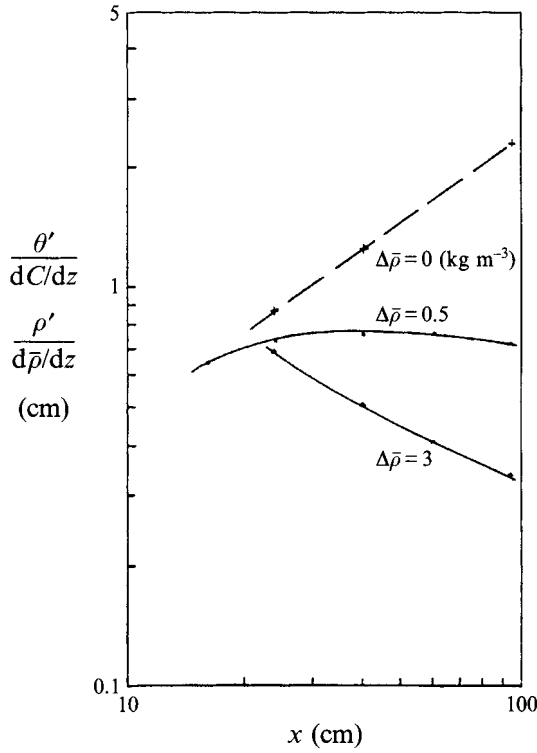


FIGURE 17. Evolution of lengthscale  $l_\rho$ .  $\theta'/(dC/dz)$  is ordinate for passive case ( $\Delta\bar{\rho} = 0$ ). Data at centre of interface,  $z = 0$ .  $S_c = 700$ .

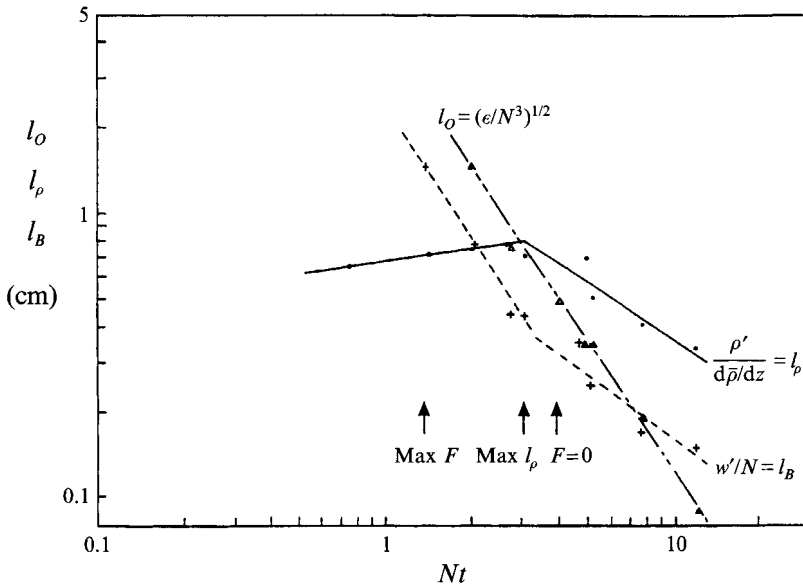


FIGURE 18. Evolution of lengthscales  $l_O$ ,  $l_\rho$ ,  $l_B$  at centre of mean interface,  $z = 0$ .  $S_c = 700$ . Arrows indicate locations of maximum normalized flux  $F$ , maximum value of lengthscale  $l_\rho$  and  $F = 0$ .

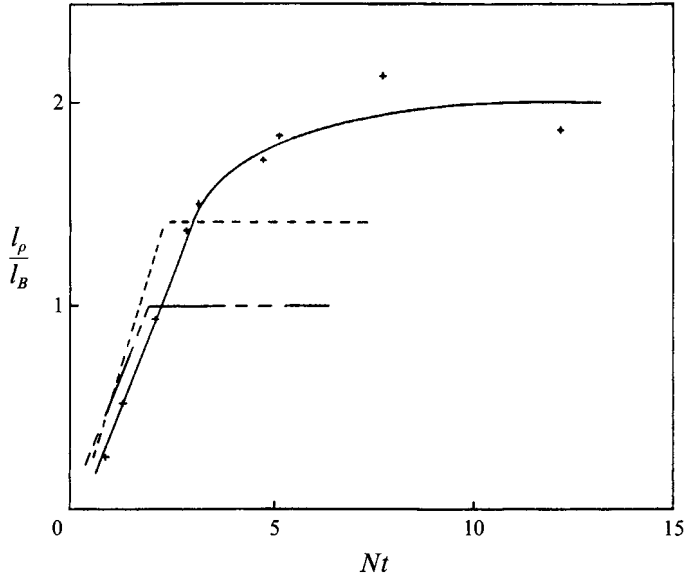


FIGURE 19. Evolution of  $l_\rho/l_B = \rho'N/[(d\bar{\rho}/dz)w']$  at centre of mean interface,  $z = 0$ .  $S_c = 700$ . Also shown are data from linearly stratified experiment of Itsweire *et al.* (1986) for which  $S_c = 700$  (-----); and the two-layer stratification experiment of Jayesh *et al.* (1991) for which  $S_c = 0.7$ . (-·-·-·).

the initial influence of stratification is to reduce flux (i.e.  $F$ ) with appreciable effects starting at  $Nt \sim 1.3$ ; similarly, mean vertical scales diminish at  $Nt \sim 3$  and so reduce  $F$  to zero at  $Nt \sim 4$ . The relative magnitude of these three lengthscales changed with the development of the flow. For  $Nt < 2$ ,  $l_\rho$  was the smallest scale;  $l_B$  was the smallest scale for  $2 < Nt < 7.5$ ;  $l_o$  was the smallest scale for  $Nt > 7.5$ . There are implications for turbulence modelling. For example, it has been suggested that the lengthscale  $l_B$  is the relevant one which determines turbulent diffusion processes (Hunt, Stretch & Britter 1988). And note that whereas all three lengthscales evolve with density stratification there is little change in the dissipation rate  $\epsilon$  between stratified and passive cases (see §4.3). This implies that the dissipation rate lengthscale is not influenced by stratification, but rather is set by initial conditions at the grid (Hunt *et al.* 1988).

The ratio of the turbulent potential energy to the vertical turbulent kinetic energy is expressed by the ratio  $l_\rho/l_B$ . Figure 19 shows the results of the present experiment together with the results from the salt-stratified linear density gradient experiment of Itsweire *et al.* (1986); for which  $S_c = 700$ , and the two-layer, thermally stratified wind tunnel experiment of Jayesh *et al.* (1991), where  $S_c = 0.7$ . Three features are evident. First, the similarity of the ratios  $l_\rho/l_B$  for the experiments for which  $S_c = 700$  further confirms that the evolution of the turbulence for the two-layer and linear stratifications are similar. Second, the ratio is not oscillatory which is unlike the numerical simulations of Riley *et al.* (1981) and Metais (1985) and the rapid distortion calculations of Stretch (1986) and Hunt *et al.* (1988). This may be attributable to the fact that the numerical simulations and rapid distortion calculations are based on idealized initial conditions which can significantly change the magnitude of oscillations, as was shown by Stretch (1986). Third, comparison of the two-layer stratification experiments show that the ratio of  $l_\rho/l_B$  is greater for  $S_c = 700$  experiments for  $Nt > 2$  thus showing the influence of the effects of molecular diffusivity.

The results of autocorrelation of the  $u$ -,  $w$ -signals (figure 20) exhibit, albeit with

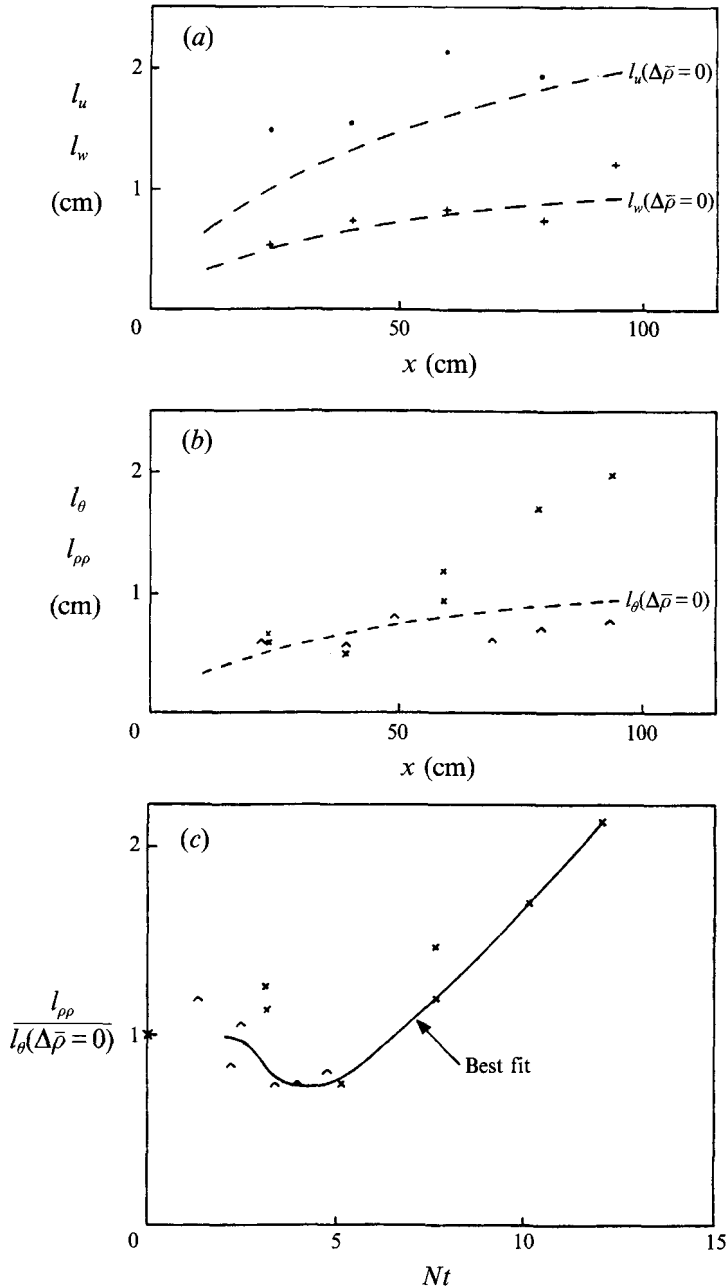


FIGURE 20. Evolution of stratified integral lengthscales from autocorrelation at centre of mean interface. (a) Longitudinal and transverse integral lengthscales from autocorrelation of  $u$  and  $w$  signals for  $\Delta\bar{\rho} = 3 \text{ kg m}^{-3}$ . Dashed lines are best fit lines of passive case ( $\Delta\bar{\rho} = 0$ ) data. (b) Scalar integral lengthscales for  $\Delta\bar{\rho} = 0.5$  ( $\wedge$ ) and  $3 \text{ kg m}^{-3}$  ( $\times$ ). Dashed line is best fit line through scalar integral scale data of passive case.  $S_c = 700$ . (c) Non-dimensional plot of scalar integral length data. Ordinate normalized by passive case values.

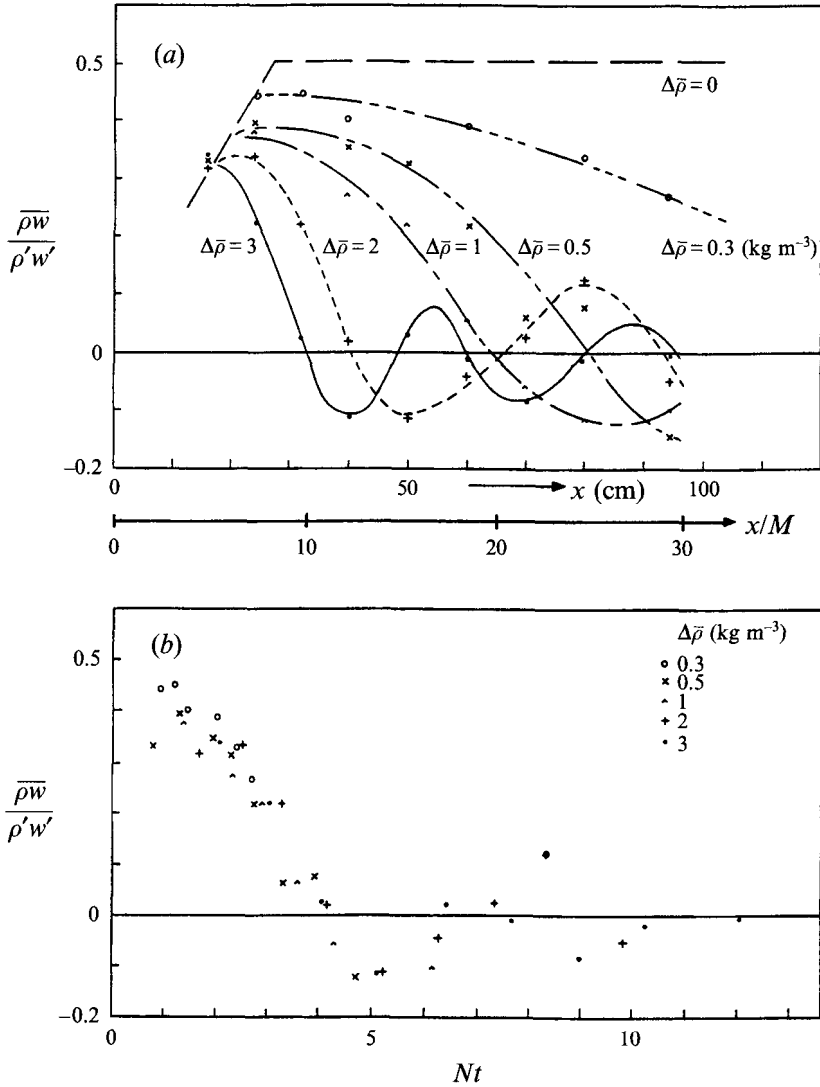


FIGURE 21. (a) Evolution of the normalized buoyancy flux at centre of mean interface for various values of  $\Delta\rho$ .  $S_c = 700$ . Note dimensional and non-dimensional abscissa. (b) As (a) but with  $Nt$  scaling.

greater scatter, the trends of the passive case; however,  $l_{\rho\rho}$ , which was obtained from autocorrelation of the  $\rho$ -signal, increases for  $Nt > 7$ , with greater correlation lengths being indicative of increased spatial uniformity. This is consistent with the interpretation of the flow visualization results of figure 1.

#### 4.5. Fluxes

The inhibiting effect of stable stratification on the normalized buoyancy flux  $F = \overline{\rho w}/\rho' w'$  is shown in figure 21(a). The measurements show that close to the grid,  $F$  approaches the passive case ( $\Delta\bar{\rho} = 0$ ) values of 0.5 for  $\Delta\bar{\rho} = 0.3 \text{ kg m}^{-3}$ ,  $R_{iM} = 0.02$ . For larger density differences the peak value of  $F$  is smaller and the decay faster. Significant negative values (i.e. counter-gradient flux) and oscillatory evolution

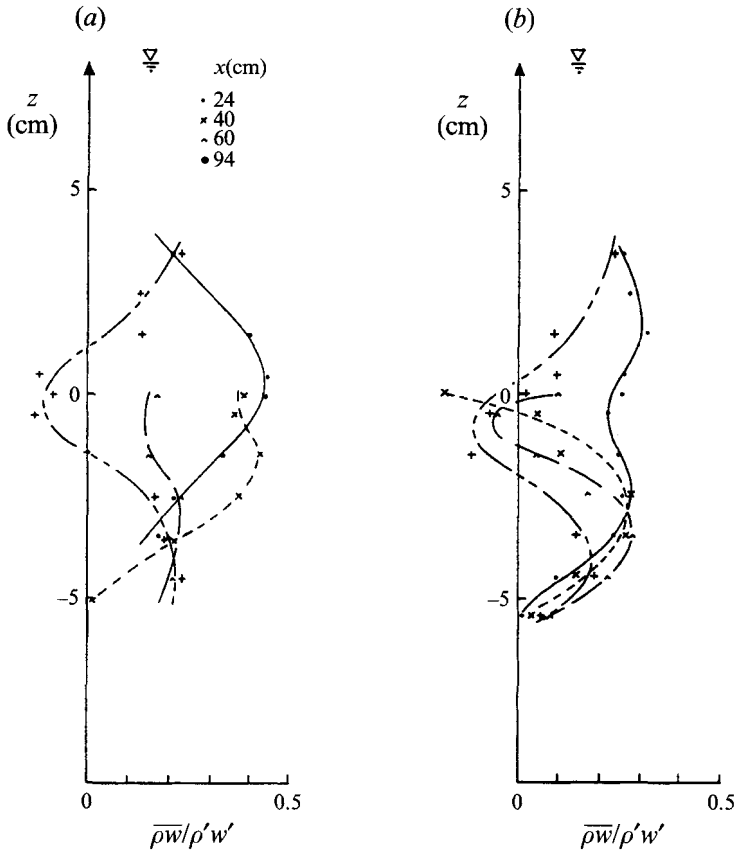


FIGURE 22. Evolution of vertical distribution of the normalized flux, for (a)  $\Delta\bar{\rho} = 0.5$  and (b)  $3 \text{ kg m}^{-3}$ .  $S_c = 700$ .

occurred for large downstream distances.  $Nt$  scaling collapses the data (figure 21 *b*) with peak values of  $F \approx 0.45$  occurring at  $Nt \approx 1$  (values similar to Itsweire *et al.* 1986),  $F = 0$  at  $Nt \approx 4$ , the maximum value  $F \approx -0.1$  of the counter-gradient flux occurring at  $Nt \approx 5$ , and  $F \approx 0$  again at  $Nt \approx 6.5$  with small oscillating values of  $F$  thereafter. For the present experiments  $S_c = 700$ , and the maximum measured values of  $F \approx 0.45$ . Jayesh *et al.* (1991) obtained maximum values of  $F \approx 0.7$  for their two-layer thermally stratified wind tunnel experiments ( $S_c = 0.7$ ). This demonstrates another effect of molecular diffusivity, namely that flux decreases with increasing  $S_c$  (the ratio of the diffusivity of momentum,  $\nu$ , to the diffusivity of the density inducing agent,  $\kappa$ ). A similar conclusion for the wholly linear density gradient experiments was found by Lienhard & Van Atta (1990). This is in accord with the observations of Turner (1968) who found that the rate of mixing (or entrainment rate) in oscillating-grid mixing box experiments was greater for density stratification induced by heat than for salt in otherwise identical turbulent velocity fields.

The evolution of the vertical distribution of  $F$  of figure 22 also demonstrates the effect of stratification – the density gradients at the interface result in smaller values of  $F$ . The magnitude of the buoyancy forces relative to the inertial forces grows with distance from the grid, and the mean density profiles evolved slowly (e.g. figure 7 shows that at the centre of the interface  $N$  is approximately constant over the length of the flume). The normalized flux profiles of figure 22 may be understood in terms of a

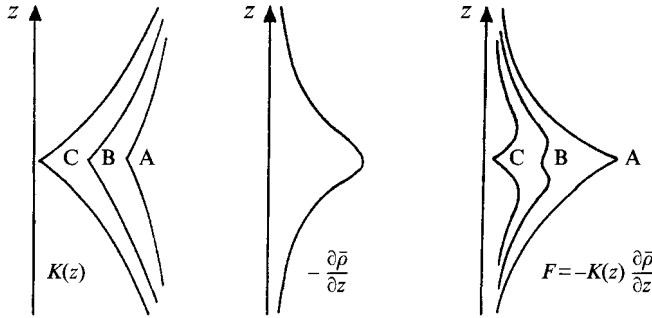


FIGURE 23. Eddy diffusivity schematization of vertical flux profiles. (A  $\rightarrow$  B  $\rightarrow$  C denotes increasing stratification or distance.) Product of vertically varying profiles of eddy diffusivity and density gradient yields profiles of flux  $F$  that are similar to the measured profiles of figure 22.

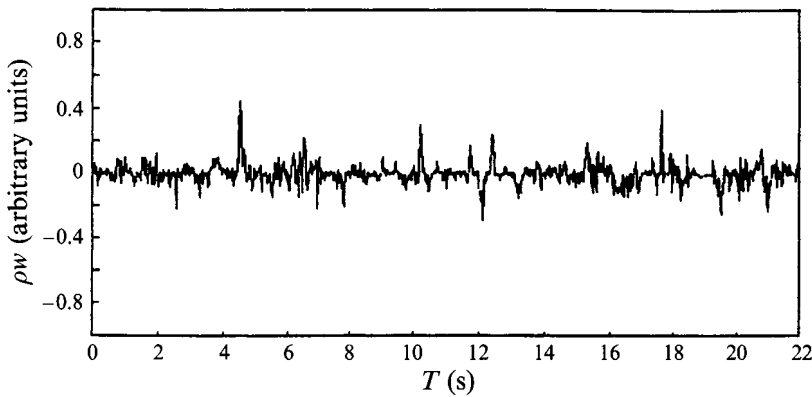


FIGURE 24. Time series of  $\rho w$  for  $Nt = 7.7$  at centre of mean interface. Both positive and negative contributions to the instantaneous flux  $\rho w$  are evident.

vertically varying eddy diffusivity  $K(z)$  varying inversely with  $N$  – see figure 23.  $K(z)$  can be deduced from a gradient transport model using the measured profiles of flux  $F$  and density gradient  $\partial\bar{\rho}/\partial z$  (i.e.  $F = K(z)\partial\bar{\rho}/\partial z$ ). Multiplying the schematic profiles of  $K(z)$  and  $\partial\bar{\rho}/\partial z$  yields a striking correspondence between the schematized and measured flux profiles. The departure from passive values of  $F (= 0.5)$  at the centre of the interface is seen to increase with distance from the grid in figure 22 in accord with the schematization of figure 23. Though the gradient transport model is useful in interpretation, its limitations should be recognized. The gradient transport or eddy diffusivity model is valid only when the characteristic scale of the turbulent transport mechanism is small compared to the lengthscale of the inhomogeneity of the mean density field. This is not the case at the interface where  $l_\rho \approx l_B \approx h$  (see figures 6 and 18). Thus the generality of the schematized forms of  $K(z)$  of figure 23 is open to question.

The data of figure 21 showed that counter-gradient transport is significant for  $Nt > 3$ . This is due to significant numbers of negative contributions to the instantaneous flux for large  $Nt$ . Figure 24 shows a typical time series of the  $\rho w$  signal for  $Nt = 7.7$ . It is evident that peak values of  $\rho w$  (i.e. significant flux events) are intermittent, and that there are approximately equal numbers of positive and negative contributions to the instantaneous flux. And so it may be expected that the value of the average flux  $F$  will be less than the value of  $F$  for the passive case. Indeed for  $Nt = 7.7$  the value of  $F \approx 0$

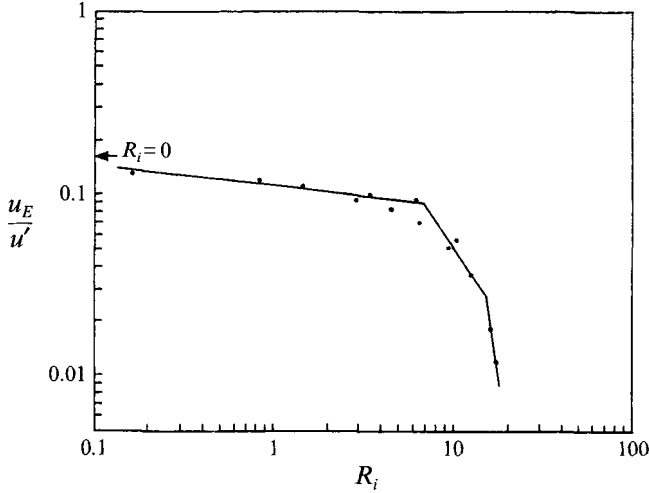


FIGURE 25. Variation of entrainment rate  $u_E/u'$  with  $R_i = g'l_u/u'^2$ .  $S_c = 700$ .

is less than the value of  $F \approx 0.5$  for the passive case (see figure 21). For the passive case there were relatively much fewer negative contributions to the instantaneous flux. Like other turbulent mixing processes flux in turbulent stratified flows is due to positive and negative contributions to the instantaneous flux, that is down-gradient and counter-gradient transport, with the ratio varying with  $Nt$ .

#### 4.6. Entrainment rate and flux Richardson numbers

Entrainment rate  $E = u_E/u'$ , where  $u_E = \overline{\rho w}/\frac{1}{2}\Delta\bar{\rho}$ , were determined from  $\overline{\rho w}$  measurements at the centre of the interface for downstream locations up to the first zero crossing of figure 21 (a). Figure 25 shows the results plotted in the form of Turner (1968) with  $R_i = g'l_u/u'^2$  ( $l_u$  is the integral scale from autocorrelation of the  $u$ -signal of the passive case, i.e.  $l_{R_{11}(r,0,0)}$ , see figure 20).  $E$  asymptotes towards the limit of the passive case value of  $E \approx 0.16$  for  $R_i < 6$ . The power law of the  $E$ - $R_i$  curve changes to approximately  $-3/2$  as buoyancy effects increase for  $R_i > 6$ , and there is a further change of slope as  $\overline{\rho w} \rightarrow 0$ . While the approximate power law of  $-3/2$  is in accord with previous results (e.g. Hannoun & List 1988) for salinity-induced buoyancy (i.e.  $S_c = 700$ ), it is different from the  $E \sim R_i^{-1}$  scaling which arises from energy arguments (Turner 1968). Thus the rate of change of potential energy ( $\sim \Delta\rho g l u_E$ ) is dependent upon the rate of energy supply ( $\sim \rho u'^3$ ) in a more complex manner than is implied in the  $E \sim R_i^{-1}$  scaling argument. The results of LIF (figure 2) showed that interfacial convolutions ( $\delta_{max}/l_u \approx 2.6$ ) attenuate as  $R_i^{-4/5}$  for stronger stratification. This suggests that suppression of vertical scales, in particular the reduced likelihood of isopycnals being rotated beyond the vertical, is the principal reason for the reduction of  $E$  with  $R_i$ .

The fraction of the available turbulent energy consumed during the mixing process, namely the flux Richardson number,

$$R_f = \frac{\int \frac{g_i}{\bar{\rho}} \overline{\rho w} dz}{\int \bar{U}_k \frac{\partial}{\partial x_k} (\frac{1}{2} \overline{q^2}) dz}$$

has been determined by integrating over the depth of the fluid. The results (figure 26)



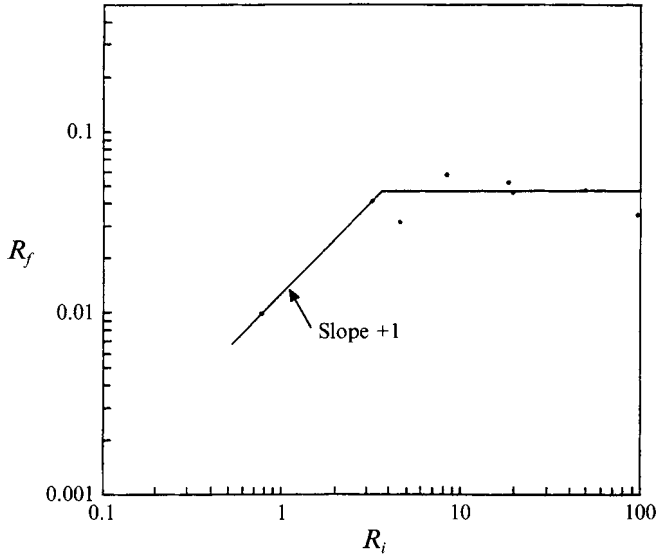


FIGURE 26. Variation of flux Richardson number  $R_f$  with  $R_i$ .  $S_c = 700$ .

show that  $R_f$  increases approximately linearly with  $R_i$  (for  $R_i = 0$  there is no change in potential energy therefore  $R_f = 0$ ) until buoyancy effects are significant (at  $R_i \approx 6$ ). Thereafter  $R_f$  maintains a constant value of  $\approx 0.05$ . The present values of  $R_f$  are smaller than the values of Thorpe (1973) of about 0.25 because of the greater availability of energy in his experiments due to local (i.e. internal) generation of turbulence by shear. The monotonic form of the  $R_f$ - $R_i$  curve is in contrast to Linden (1980) who found that  $R_f$  decreased for large  $R_i$ . However, Linden assumed the available energy input from the free-falling grid in a mixing box configuration to be independent of the density difference which is not justifiable *a priori*, or in the light of the dependency of  $R_f$  on  $S_c$  (e.g. for  $S_c \rightarrow 0$ ,  $R_f \rightarrow 1$ , conversely  $R_f \rightarrow 0$  for  $S_c \rightarrow \infty$  for the same energy input). The present stepwise configuration suffers from an unavoidable uncertainty as to the vertical extent of energy input involved in mixing, but the concurrent flux and velocity measurements make unnecessary *a priori* assumptions about the influence of stratification on the velocity field. The increase in  $R_f$  is arrested at  $R_i \approx 6$  as buoyancy effects become significant. Note that the  $E$ - $R_i$  curve attenuates to  $E \sim R_i^{-1.5}$  at  $R_i \sim 6$ , and also that  $\delta_{max}/l_u$  changes similarly at  $R_i \sim 6$ . The near constancy of  $R_f$  for large  $R_i$ , even though  $F$  may be negative at the interface centre, is due to the vertical redistribution of previously entrained fluid -  $F$  is positive away from the interface (figure 22). Such redistribution (which sharpens the interface, see figures 1 and 6) is not possible in a wholly linearly stratified fluid column. In that case  $R_f$  will decrease from a peak value for large  $R_i$  as the flow is still dissipative (Rohr, Itsweire & Van Atta 1984). It is clear that the  $R_f$ - $R_i$  variation is more complex than anticipated, and it depends on the whole profile, molecular diffusivities and the character (internal or externally generated turbulence) of the energy source.

## 5. Summary and conclusions

To study the evolution of decaying grid-generated turbulence and mixing in stratified fluids a series of experiments with two homogeneous layers of differing densities, stably stratified, co-flowing without shear were conducted in a purpose built,

low noise water tunnel. Density stratification was induced by salinity ( $S_c = 700$ ) and results compared with the passive case (the case without a density difference but with a marked scalar in one layer, i.e.  $\Delta\bar{\rho} = 0$ ) of Huq & Britter (1995).

Relative to the passive case the effect of density stratification is to attenuate turbulent velocity fluctuations, vertical motions and interfacial convolutions, normalized density fluctuations ( $\rho'/\Delta\bar{\rho}$ ), flux  $\overline{\rho w}$  and mean interfacial thickness. LIF shows that large density difference interfaces are more quiescent and engulfment events more rare. Within an integral length of the centreline of the interface, distortion of eddies by interaction with the flapping instantaneous interface amplifies the lateral velocity components so that  $u'$  can be greater than passive case values. Vertical velocity fluctuations increase monotonically away from the interface whereas the  $u'$  distribution can be non-monotonic. The evolution of density fluctuations differs markedly from passive scalar fluctuations as the growth of fluctuations is arrested when buoyancy forces dominate. Results indicate that stratification reduces the flux  $\overline{\rho w}$  at  $Nt \sim 1.3$ , mean vertical scales at  $Nt \sim 3$ , and decreases  $\overline{\rho w}$  to zero at  $Nt \sim 4$ . Lengthscales  $l_\rho, l_B, l_o$  evolved with the flow, with the relative magnitudes varying with  $Nt$ .

Flux in stratified flows is a combination of down-gradient and counter-gradient transport (the ratio varying with  $Nt$ , e.g. at  $Nt \sim 5$  the flux is counter-gradient). For the present experiments for which  $S_c = 700$ , the maximum value of non-dimensional flux was found to be about 0.5, which is less than the value of about 0.7 typical of thermally stratified wind tunnel experiments for which  $S_c = 0.7$ . The flux Richardson number  $R_f$  was found to increase monotonically to a value of  $\sim 0.05$ .

We would like to thank D. J. Carruthers, Professor J. C. R. Hunt FRS, and D. D. Stretch for their encouragement and critical discussions throughout this work. Financial support from British Gas plc in the form of an Engineering Research Award to P.H. is gratefully acknowledged.

#### REFERENCES

- CARRUTHERS, D. J. & HUNT, J. C. R. 1986 Velocity fluctuations near an interface between a turbulent region and a stably stratified layer. *J. Fluid Mech.* **165**, 475–501.
- CHAMPAGNE, F. H. & SLEICHER, C. A. 1967 Turbulence measurements with inclined hot wires. *J. Fluid Mech.* **28**, 177–182.
- CSANADY, G. T. 1964 Turbulent diffusion in a stratified fluid. *J. Atmos. Sci.* **21**, 439–447.
- CSANADY, G. T. 1973 *Turbulent Diffusion in the Environment*. D. Reidel.
- ELLISON, T. H. 1957 Turbulent transport of heat and momentum from an infinite rough plane. *J. Fluid Mech.* **2**, 456–466.
- HANNOUN, I. A., FERNANDO, H. J. & LIST, E. J. 1988 Turbulence structure near a sharp density interface. *J. Fluid Mech.* **189**, 189–209.
- HANNOUN, I. A. & LIST, E. J. 1988 Turbulent mixing at a shear-free density interface. *J. Fluid Mech.* **189**, 211–234.
- HOLLIDAY, D. & MCINTYRE, M. E. 1981 On potential energy density in an incompressible, stratified fluid. *J. Fluid Mech.* **107**, 221–225.
- HUNT, J. C. R., STRETCH, D. D. & BRITTER, R. E. 1988 Length scales in stably stratified turbulent flows and their use in turbulence models. In *Stably Stratified Flows and Dense Gas Dispersion* (ed. J. S. Puttock), pp. 285–321. Clarendon Press.
- HUQ, P. 1990 Turbulence and mixing in stratified fluids. PhD dissertation, University of Cambridge.
- HUQ, P. & BRITTER, R. E. 1995 Mixing due to grid-generated turbulence of a two-layer scalar profile. *J. Fluid Mech.* **285**, 17–40.
- ITSWEIRE, E. C., HELLAND, K. N. & VAN ATTA, C. W. 1986 The evolution of grid-generated turbulence in a stably stratified fluid. *J. Fluid Mech.* **162**, 299–338.

- JAYESH, YOON, K. & WARHAFT, Z. 1991 Turbulent mixing and transport in a thermally stratified layer formed in decaying grid turbulence. *Phys. Fluids A* **3**, 1143–1155.
- LAWSON, R. E. & BRITTER, R. E. 1983 A note on the measurements of transverse velocity fluctuations with heated cylindrical sensors at small mean velocities. *J. Phys. E: Sci. Instrum.* **16**, 563–567.
- LIENHARD, J. H. & VAN ATTA, C. W. 1990 The decay of turbulence in thermally stratified flow. *J. Fluid Mech.* **210**, 57–112.
- LINDEN, P. F. 1980 Mixing across a density interface produced by grid turbulence. *J. Fluid Mech.* **100**, 691–703.
- MCDUGALL, T. J. 1979 Measurements of turbulence in a zero-mean-shear mixed layer. *J. Fluid Mech.* **94**, 409–431.
- METAIS, O. 1985 Evolution of three dimensional turbulence under stratification. In *5th Symp. on Turbulent Shear Flows*, Cornell.
- PEARSON, H. J., PUTTOCK, J. S. & HUNT, J. C. R. 1983 A statistical model of fluid element motions and vertical diffusion in a homogeneous stratified turbulent flow. *J. Fluid Mech.* **129**, 219–249.
- RILEY, J. J. 1985 A review of turbulence in stably-stratified fluids. *7th Symp. on Turbulence and Diffusion*, *Am. Met. Soc.*
- RILEY, J. J., METCALFE, R. W. & WEISSMAN, M. A. 1981 Direct numerical simulations of homogeneous turbulence in density-stratified fluids. In *Non-linear Properties of Internal Waves*. AIP Conf. Proc. 76.
- ROHR, J. J., ITSWEIRE, E. C. & VAN ATTA, C. W. 1984 Mixing efficiency in stably-stratified decaying turbulence. *Geophys. Astrophys. Fluid Dyn.* **29**, 221–236.
- SREENIVASAN, K. R., TAVOULARIS, S., HENRY, R. & CORRISIN, S. 1980 Temperature fluctuations and scales in grid-generated turbulence. *J. Fluid Mech.* **100**, 597–621.
- STRETCH, D. D. 1986 The dispersion of slightly dense contaminants in a turbulent boundary layer. PhD dissertation, University of Cambridge.
- TENNEKES, H. & LUMLEY, J. L. 1982 *A First Course in Turbulence*, 2nd Edn. MIT Press.
- THOMAS, N. H. & HANCOCK, P. E. 1977 Grid turbulence near a moving wall. *J. Fluid Mech.* **82**, 481–496.
- THORPE, S. A. 1973 Experiments on instability and turbulence in a stratified shear flow. *J. Fluid Mech.* **61**, 731–751.
- TOWNSEND, A. A. 1958 The effects of radiative transfer on turbulent flow of a stratified fluid. *J. Fluid Mech.* **4**, 361–375.
- TURNER, J. S. 1968 The influence of molecular diffusivity on turbulent entrainment across a density interface. *J. Fluid Mech.* **33**, 639–656.
- TURNER, J. S. 1973 *Buoyancy Effects in Fluids*. Cambridge University Press.
- WARHAFT, Z. & LUMLEY, J. L. 1978 An experimental study of the decay of temperature fluctuations in grid-generated turbulence. *J. Fluid Mech.* **88**, 659–684.
- YOON, K. & WARHAFT, Z. 1990 The evolution of grid-generated turbulence under conditions of stable thermal stratification. *J. Fluid Mech.* **215**, 601–638.